Seasonal changes in metal and nutrient fluxes across the sediment-water interface in tropical mangrove creeks in the Amazon region

Christiene R.L. Matos, José Berrêdo, Wilson Machado, Édouard Metzger, Christian Sanders, Kelson C.F. Faial, Marcelo C.L. Cohen

Seasonal changes in metal and nutrient fluxes across the sediment-water interface in tropical mangrove creeks in the Amazon region

Christiene R. L. Matos[a,*], José F. Berrêdo[a,], Wilson Machado[b], Edouard Metzger[c], Christian J. Sanders[d], Kelson C. F. Faial[e], Marcelo C. L. Cohen[f]

[a]Museu Paraense Emílio Goeldi/MCTIC. Belém, Pará, Brazil.

[b]Programa de Pós-Graduação em Geoquímica, Universidade Federal Fluminense, Niterói, Rio de Janeiro, Brazil.

[c]Laboratoire des Bio-Indicateurs Actuels et Fossiles, UMR6112 CNRS LPG-BIAF, Université d'Angers, Angers, France.

[d]National Marine Science Centre, Southern Cross University, Coffs Harbour, New South Wales, Australia.

[e]Laboratório de Toxicologia, Seção de Meio Ambiente, Instituto Evandro Chagas, Belém, Pará, Brazil

[f]Programa de Pós-Graduação em Geologia e Geoquímica, Universidade Federal do Pará, Belém, Pará, Brazil.

*Corresponding author at: Museu Paraense Emílio Goeldi, Av. Perimetral, 1901 – CEP. 66077-830, Belém – Pará, Brazil.

E-mail addresses: christienematos@hotmail.com (C.R.L. Matos), berredo@museu-goeldi.br (J.F. Berredo), wmachado@geoq.uff.br (W. Machado), edouard.metzger@univ-angers.fr (E. Metzger), christian.sanders@scu.edu.au (C.J. Sanders), kelsonfaial@iec.gov.br (K.C.F. Faial), mcohen80@hotmail.com (M.C.L. Cohen).

ABSTRACT

Mangrove creeks are considered important routes between terrestrial and adjacent coastal waters regarding the transport of dissolved material to oceans. The present study assessed if Amazonian seasonal rainfall patterns affect the pore water biogeochemistry and the intensity and direction of nutrient (NH_4^+ and PO_4^{3-}) and metal (Fe^{2+} and Mn^{2+}) exchanges from intertidal creek mudflats fringed by pristine mangroves. The results indicate that mangrove-fringed mudflats are effective in retaining iron and nutrients in solid sediment phases compared to export to coastal waters, also potentially comprising a significant manganese contributor to coastal waters. However, nutrient and metal retention are lower during the wet season, as intense rainfall periods reduce pore water salinity and promote increased reducing sediment conditions. Such conditions enhance organic matter degradation and pore water NH_4^+, PO_4^{3-}, Fe^{2+} and Mn^{2+} concentrations just below the sediment-water interface, generating higher effluxes during this period. Our findings demonstrate that seasonal variabilities drive substantial physicochemical property and pore water biogeochemistry changes, affecting the efficiency of mudflat sediments retaining and exporting nutrients and metals.

Keywords: Seasonal variations. Intertidal environmental. Organic matter degradation. Pore water exchange. Sediment-water interface.

1 Introduction

Mangroves occur along the land-ocean interface under the influence of both fresh and seawater. These ecosystems, whether pristine or disturbed, can act as sinks and store significant amounts of carbon (Alongi, 2020a), nutrients (Breithaupt et al., 2014; Sanders et al., 2014) and metals (Marchand et al., 2011; Thanh-Nho et al., 2019) in their sediments. Alternatively, mangroves may also play an essential role in exchanging of dissolved and particulate matter between terrestrial and oceanic environments (Dittmar et al., 2006; Jennerjahn and Ittekkot, 2002). The capacity of mangrove systems to act as net sinks or sources of nutrient and metal is influenced by many factors, including the input of terrestrial or oceanic nutrients, shifts in redox conditions, anthropogenic activities, and local environmental factors such as weather conditions, hydrology, tidal range, latitude, mangrove community structure and topographic elevation (Adame et al., 2010; Adame and Lovelock, 2011; Kristensen et al., 2017).

Mangrove creeks are considered important routes between forest environments and adjacent coastal waters regarding the transport of dissolved and suspended materials (Dittmar and Lara, 2001; Lacerda et al., 1999). However, mangrove sediment creeks also can act as biogeochemical reactors, and their pore water can become a crucial source of dissolved metals and nutrients to coastal areas, if these elements are not efficiently removed from pore waters by precipitation and sorption processes in the upper sediment layers (Ogrinc and Faganeli, 2006; Rozan et al., 2002). These dissolved elements exchange can take place essentially by spontaneous molecular diffusion across the sediment-water interface (SWI) including in macrotidal regimes (Alongi et al., 2004; Bally et al., 2004; Pan et al., 2020; Pratihary et al., 2021; Thibault de Chanvalon et al., 2017; Wang et al., 2011), through pore water seepage into tidal creek water columns during low and ebbing tides (Holloway et al., 2016; Sanders et al., 2015; Taillardat et al., 2019; Tait et al., 2017) or transported by bioturbation (irrigation from burrows and biodiffusion) (Bouillon et al., 2007; Ovalle et al., 1990).

In addition to tides, regional seasonality also influences estuarine water quality. Mangroves developed under the Amazon hydrological regime, for example, are subject to high annual rainfall rates which, in turn, lead to high seasonal freshwater inputs and fluvial water discharges, causing extreme salinity fluctuations within estuaries and tidal creeks. Therefore, the biogeochemistry of these waters alter at both the temporal (seasonal, tidal, diel) and spatial scales, due to seasonal fluvial discharge and organic matter (OM) input from different sources (mainly mangroves and phytoplankton). Previous assessments have reported that the documented seasonal rainfall patterns can lead to seasonal changes in sedimentary physical and chemical properties (Alongi et al., 2004; Berrêdo et al., 2016; Marchand et al., 2004) pore water chemistry (Lee et al., 2008; Taillardat et al., 2019; Thanh-Nho et al., 2020; Wu et al., 2015) and nutrient and metals fluxes to coastal waters (Adame et al., 2010; Alongi et al., 2001; Rao et al., 2018; Yasui et al., 2016). Therefore, local weather conditions in the estimation and management of nutrient and metal budgets, especially in small mangrove rivers (Terada et al., 2017), must be considered.

In the present study, Amazonian seasonal rainfall patterns are hypothesized to significant affect the physicochemical properties and pore water biogeochemistry of creek mudflats, as well as metal and nutrient fluxes at the SWI. To assess rainfall effects on creek mudflats sediment and pore water dynamics, field observations were conducted in three intertidal mudflat sediments fringed by pristine mangroves in the Marapanim River Estuary (MRE), northern Brazil, in both the wet (April 2017) and dry (September 2017) seasons. To this end, the temporal and spatial distributions of pH, Eh, salinity, Cl^-, SO_4^{2-}, Fe^{2+}, Mn^{2+}, total alkalinity (TA) and nutrients (NH_4^+ and PO_4^{3-}) were first obtained alongside sediment parameters. Diffusive nutrient and metal fluxes between sediment pore waters and the overlying water were subsequently estimated. Finally, rainfall effects on the physicochemical conditions, pore water biogeochemistry and nutrient and metal fluxes at the SWI, and the importance of the creek mudflats to coastal biogeochemical cycles were then assessed.

2 Materials and methods

2.1 Study area

The MRE, located in the state of Pará, northern Brazil (00º30’ to 01º00’S and 47º32’ to 47º00’W, Fig. 1), can be subdivided into three morphologic realms, namely the coastal, estuarine and alluvial plains (Silva et al., 2009). The sedimentary deposits of the Coastal Plateau are represented by cliffs and lateritic soils (Pleistocene) derived from the Barreiras Formation (Tertiary), the main source of sand, silt and clay fractions, comprising quartz, clay minerals (kaolinite and illite), iron oxides, and recent sediments (Holocene) that constitute mangrove substrates (Berrêdo et al., 2008a). The estuarine plain where mangroves are established presents sandy and muddy deposits (Silva et al., 2009).

The tidal flats of the MRE are occupied by well-developed mangroves, which are part of the largest continuous and best-preserved mangrove forest in the world (Kauffman et al., 2018; Nascimento et al., 2013). The main river channel is about 70 and 8 km long and wide at the mouth, presenting the incursion of oceanic waves from Atlantic and semi-diurnal macrotides that present a tidal range of 3.5 m during neap tides and over 6 m during spring tides (Silva et al., 2009). Saline waters penetrate approximately 62 km up the main river channel during the dry season and 42 km during the wet season (Berrêdo et al., 2008b).

The coastal region of Pará is characterized by a tropical climate with two distinct seasons. The wet season occurs between January and June, when total rainfall often exceeds 2000 mm, with a mean April rainfall of 462 mm. The dry season ranges from July to December, with a mean September rainfall of 5 mm. The annual mean temperature is 27.7 ºC. The estuary water temperature ranges from 27 to 30 ºC. The pH values along the estuarine channel range between alkaline (7.9 to 8.0) to slightly acidic (5.7 to 6.7) during the dry and wet seasons, respectively (Berrêdo 2008b).

118 The samplings were carried out along three intertidal mudflats, numbered according to their
119 distance from the main Marapanim River, with number 1 (P1) comprising the Marapanim River
120 margin, and numberr 2 (P2) and 3 (P3) located at two tidal mangrove creeks along the Marapanim
121 mangrove forest (Fig. 1). Sites P1 and P2 are 2.3 km apart, while site P3 is located ~1 km from P2.
122 The tidal creeks do not receive any direct freshwater inputs except for rainwater and runoff from the
123 Marapanim River during the wet season. They exhibit sinuous bifurcated forms, are shallow (3 m in
124 depth), about 5 km long and 800 m wide, and are under the influence of the semidiurnal tide regime,
125 with 6 hours intervals between the ebb and flood tides. The three sampling sites are frequently
126 exposed during the low tide.

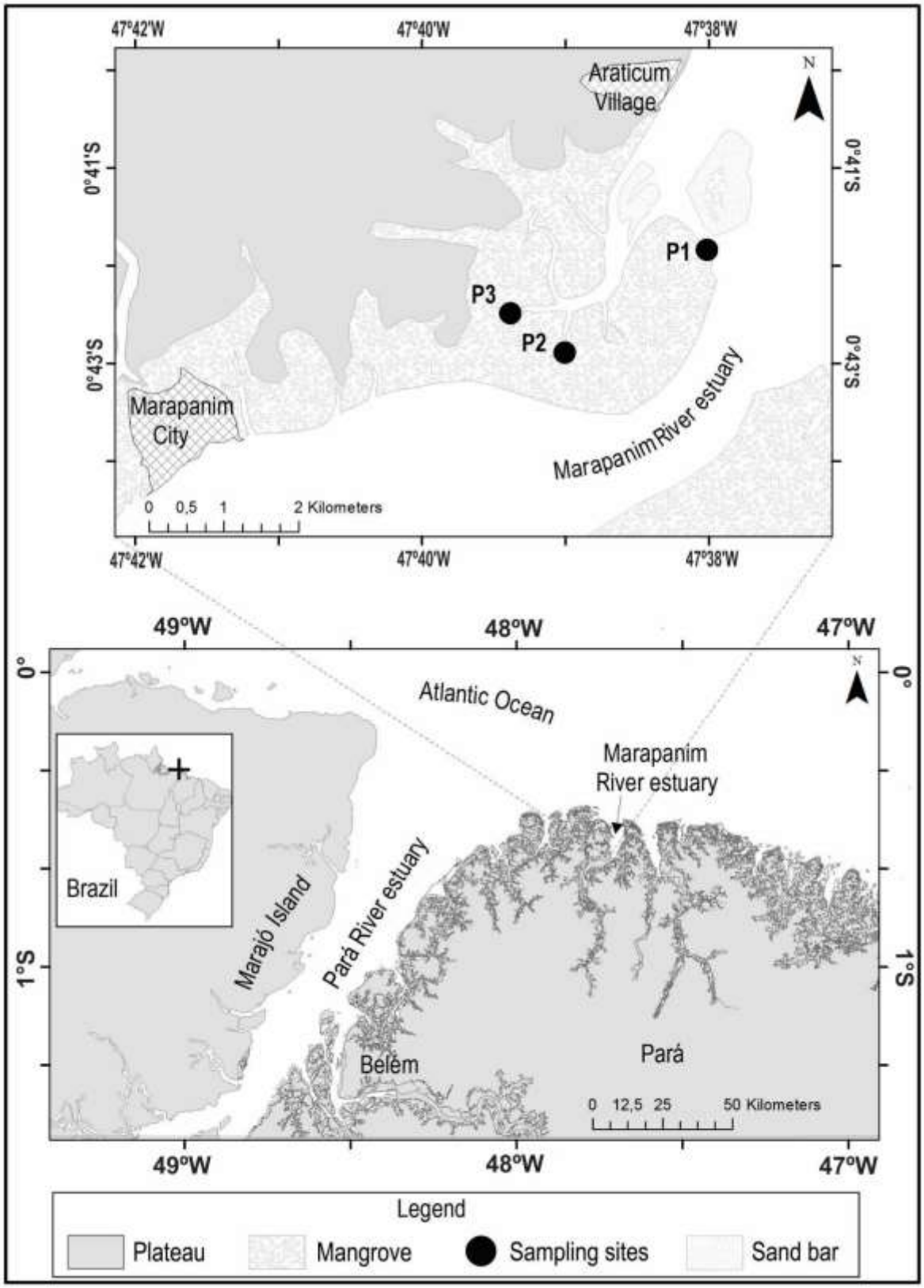

Fig. 1. Map displaying the Marapanim estuary study area, in the state of Pará, Brazil, indicating the P1, P2 and P3 sampling sites.

131

132 *2.2 Solid-phase sediment sampling and analyses*

133

134 To assess the effects of contrasting seasons, two replicate cores were collected from the
135 intertidal mudflat at each site, during the wet (April 2017) and dry (September 2017) seasons. Acrylic
136 tubes (50 cm length, 8 cm diameter) were used to recover approximately 35 cm of sediment and 15
137 cm of overlying water at a water column depth of ~0.8 m. One core, dedicated to solid-phase analyses,
138 was sliced at 1-cm (0 – 6 cm), 2-cm (6 – 20 cm), and 5-cm intervals (20 – 35 cm depth). The sub-
139 samples were stored in polyethylene bags at 4 °C until processing. An aliquot of humid sediment was
140 fixed with Zn-acetate, within a N_2-filled glove bag, for the determinations of acid volatile sulfides
141 (AVS, mainly Fe monosulfide/FeS) and chromium reducible sulfur (CRS, mainly pyrite/FeS_2).
142 The most reactive Fe (Fe_R) and Mn (Mn_R) fractions were determined using the ascorbate
143 reagent (50 g $NaHCO_3$, 50 g Na-citrate, 20 g ascorbic acid to a 1 L solution, buffered at pH 8)
144 (Anschutz et al., 2005; Kostka and Luther, 1994). Extractions were carried out using 500 mg of dried
145 sediment in 10 mL of N_2-degassed ascorbate reagent for 24 h under continuous shaking. The
146 supernatant was diluted 10-fold with HNO_3 (1.0 %), and Fe and Mn concentrations were determined
147 by atomic absorption spectrometry using an external standard prepared in the same matrix. Total
148 organic carbon (TOC) depth profiles were obtained from Matos et al., (2020). AVS and CRS were
149 determined in 1 g of sediment by a two-step distillation with cold 6 N HCl followed by boiling 2 N
150 acidic $CrCl_2$ solution (Fossing and Jørgensen, 1989). The liberated H_2S was collected in Zn-acetate
151 (20%) traps, and its concentration was determined according to the method of Cline, (1969). Scanning
152 electron microscopy (SEM) coupled with an energy dispersive X-ray spectrometer was used on
153 particles collected from sediments.

154

155 *2.3 Pore water sampling and analyses*

Regarding the second replicate core, pH and redox potential (Eh) were measured with a pH meter electrode (Metrohm 826 pH mobile) directly in the sediment through holes in one specific predrilled tube, in the same intervals as in the solid-phase, which were covered with tape during the sampling. After determining the redox-pH, following the same intervals, the overlying and pore waters were removed using Rhyzon® collectors (7 cm and 0.1 μm in length and pore diameter, respectively), inserted directly into the sediment through pre-drilled holes along the acrylic tubes (Seeberg-Elverfeldt et al., 2005). The overlying water sampling comprised ~5 cm above the SWI.

The pore water samples were treated in a N_2-filled glove bag to prevent oxidation. The overlying and pore water samples were analyzed concerning Cl^-, SO_4^{2-}, Fe^{2+}, Mn^{2+}, total alkalinity (TA), NH_4^+ and PO_4^{3-} and total dissolved sulfide ($\Sigma H_2S = H_2S + HS^- + S_0 + S_x^{-2}$). A total of 2 mL of water samples were deposited in amber vials for the alkalinity analyses. Subsamples (1 mL) were preserved in Eppendorf tubes using 100 μL of a 5% Zn-acetate solution and 10 μL HCl for the ΣH_2S and PO_4^{3-}analyses, respectively. Samples (1 mL) were preserved in Eppendorf tubes for the SO_4^{2-} and Cl^- analyses. All samples were maintained at 4 °C. Other sub-samples (1 mL) were frozen in amber vials for subsequent NH_4^+ analyses.

Dissolved Fe and Mn concentrations were determined employing an ICP-OES (VISTA-MPX CCD Simultaneous) using 10-fold dilutions. Accuracies were checked using a natural water reference NIST (1640a, 1643e), and were within 5% for Fe and Mn. TA was determined thought potentiometric Gran titration using 0.01 mol L^{-1} HCl immediately after vial removal from the glove-bag. Standard colorimetric methods were used to determine the NH_4^+ and PO_4^{3-} concentrations (Gieskes et al., 1991). ΣH_2S concentrations were quantified through the colorimetric method as proposed by Cline, (1969). The SO_4^{2-} and Cl^- concentrations of were measured by ion chromatography (Dionex DX 120) applying a 500-fold dilution. Salinity was determined using a portable refractometer (Atago).

181 *2.4 Sulfate depletion calculation*

182

183 Chloride is a conservative element, as it is not affected by biological or chemical processes.
184 It was therefore, employed to evaluate sulfate depletion ($SO_4^{2-}{}_{Dep}$) under freshwater dilution and
185 microbial removal effects. Sulfate concentrations were normalized according to chloride
186 concentration changes, according to Eq. 1:

187

188 $$(SO_4^{2-})_{Dep} = \left[\left(Cl^-{}_{pw}\right).(R_{sw})^{-1}\right] - (SO_4^{2-})_{pw} \quad (1)$$

189

190 where $(SO_4^{2-})_{Dep}$ comprised SO_4^{2-} depletion, $(Cl^-)_{PW}$ and $(SO_4^{2-})_{PW}$ consists in the pore water
191 concentrations of Cl^- and SO_4^{2-}, and R_{SW} is the molar ratio of Cl^- to SO_4^{2-} in surface seawater (R_{SW} =
192 19.33; Weston et al. 2006). Sulfate depletion reveals the net consumption of microbially mediated of
193 SO_4^{2-} (Weston et al., 2006).

194

195 *2.5 Metal and nutrient flux estimations*

196

197 The diffusive metal and nutrient flux estimates between sediment pore waters and the
198 overlying water were calculated from the interfacial concentration gradients, according to Fick's first
199 law of diffusion (Berner, 1980) below:

200

201 $$F = -\emptyset\, D_s(\Delta C/\Delta Z) \quad (2)$$

202

203 where F (mmol.m^{-2}.d^{-1}) is the diffusive flux, $\emptyset$ (dimensionless) is the porosity at the sediment
204 surface (depth = 0-1 cm), D_s (m^2.s^{-1}) is the molecular diffusion coefficient in sediment, and $\Delta C/\Delta Z$
205 comprises the concentration gradient across the SWI. According to these calculations, negative fluxes

reflect sediment uptake processes (*i.e.*, downward fluxes), whereas positive fluxes indicate benthic recycling (*i.e.*, outward fluxes to overlying waters). Porosity was expressed and calculated as the water volume fraction in the wet sediment, which was identified by the weight difference between wet sediment samples before and after drying at 60 °C. $\Delta C/\Delta Z$ consists in the concentration gradient in the overlying water and pore water. The diffusion coefficient (D_s) was calculated from the molecular diffusion coefficient in free water D_0 corrected for sediment porosity and temperature (Li and Gregory, 1974). The upper sediment layers presented porosities between 0.51 and 0.76, and overlying waters ranged between 28.0 and 29.3 °C.

2.6 Statistical analyses

Statistical assessments were carried out using the statistical package PAST version 3.26 (Hammer et al., 2001). Potential differences regarding dissolved and solid-phase concentrations between the sampling sites (P1, P2, and P3) and seasons (wet and dry) were assessed by a variance analysis (ANOVA). Data distribution normality of was first verified applying Shapiro-Wilk. Non normally distributed variables were log-transformed to fit a normal distribution. A statistical significance of $\alpha < 0.05$ was used for all statistical analyses. Pearson's correlation coefficient was employed to determine the strength of the associations between each pair of variables, where correlation coefficients higher than 0.5 were interpreted as significant.

3 Results

3.1 Sediment geochemistry

Sedimentary compositions and OM sources at each sampling site were previously characterized by Matos et al., (2020), and the mean values ± standard deviations are presented in Table 1. The estuarine mudflat (P1) presented very different sedimentary characteristics compared to the creek mudflats (P2 and P3). Located in the lowest topographic area, P1 exhibited a slightly higher sedimentation rate (1.8 cm yr^{-1}). Its grain size, however, is represented by a higher sand content (~ 52%) and significant contributions from marine OM (wet: 76.4% and dry: 79.6%). Both P2 and P3 are located in topographically higher tidal flats (~ 2 m amsl), where sediments are strongly oxidized during the dry season. The P2 site is located in a more confined area, presenting a lower sedimentation rate of 1.3 cm yr^{-1}, finer grain size of ~ 68% (silte+clay) and marine OM contributions of 54.5% in the wet season and 69% in the dry season. The P3 site, located closer to the mainland, presented a sedimentation rate of 1.5 cm yr^{-1}, finer particle size of ~ 66% and marine OM contributions of 60% in the wet season and 78% in the dry season.

Table 1

Sedimentary characteristics of the P1, P2 and P3 sampling sites, during the wet and dry seasons.

Properties	P1		P2		P3		References
	Wet	Dry	Wet	Dry	Wet	Dry	
FeR (%)	0.25 ± 0.6	0.29 ± 0.8	0.59 ± 0.11	0.54 ± 0.14	0.63 ± 0.18	0.48 ± 0.07	This study
MnR (%)	0.016 ± 0.003	0.007 ± 0.003	0.029 ± 0.006	0.016 ± 0.005	0.030 ± 0.011	0.020 ± 0.003	
TOC (%)	0.9 ± 0.3	1.3 ± 0.2	3.4 ± 0.3	2.6 ± 0.2	2.7 ± 0.2	2.5 ± 0.2	Matos et al. (2020)
Sand (%)	51.7 ± 10.4	52.6 ± 5.6	36.8 ± 7.4	26.5 ± 7.7	32.4 ± 10.3	35.6 ± 8.9	
Silt (%)	46 ± 9.3	46.3 ± 5.3	58 ± 6.6	71.5 ± 6.9	60.2 ± 9.3	62.2 ± 8.6	
Clay (%)	2.3 ± 1.3	1.0 ± 0.4	5.2 ± 1.0	2.0 ± 1.0	7.4 ± 1.5	2.2 ± 0.5	
OM_{terr} (%)	23.6 ± 6.0	20.4 ± 6.2	45.5 ± 3.4	31.0 ± 9.5	40.1 ± 3.9	21.8 ± 8.7	
OM_{mar} (%)	76.4 ± 6.0	79.6 ± 6.2	54.5 ± 3.4	69.0 ± 9.5	59.9 ± 3.9	78.2 ± 8.7	
SAR ($cm.yr^{-1}$)	1.8		1.3		1.5		

Sediment-depth profiles of TOC, FeS_2, Fe_R and Mn_R in different seasons are presented in Fig. 2, and the mean values ± standard deviation are displayed in Table 1. Sediment concentrations were different between sites, seasons, and depth. Overall, the TOC, FeS_2, Fe_R and Mn_R ranges were lower

at site P1 compared to the sites P2 and P3. At all three sites, TOC concentrations decreased slightly with depth, ranging from 3.84 to 0.53 %. FeS_2 content showed large fluctuations between the sites and seasons varying from 0.06 to 1.52 %, with the highest concentrations during the wet season. AVS concentrations were below the detection limit (<0.01 wt%) in all sediment profiles. At P1, Fe_R concentrations in both seasons decreased slightly with depth, varying from 0.43 to 0.11 %. At P2 and P3, Fe_R and Mn_R concentrations presented a clear seasonal trend, with the lowest Fe_R concentrations (0.34 % at -16 cm to P2 and 0.34 % at -8 cm to P3) determined during the wet season, and the highest concentrations (0.76 % at -16 cm to P2 and 1.07 % at -8 cm to P3) found in the dry. Mn_R concentrations ranged from 0.004 to 0.061 %, and presented almost the same depth distribution patterns as Fe_R, with one peak of 0.044 % at -20 cm to P2 and another of 0.061 % at -8 cm to P3.

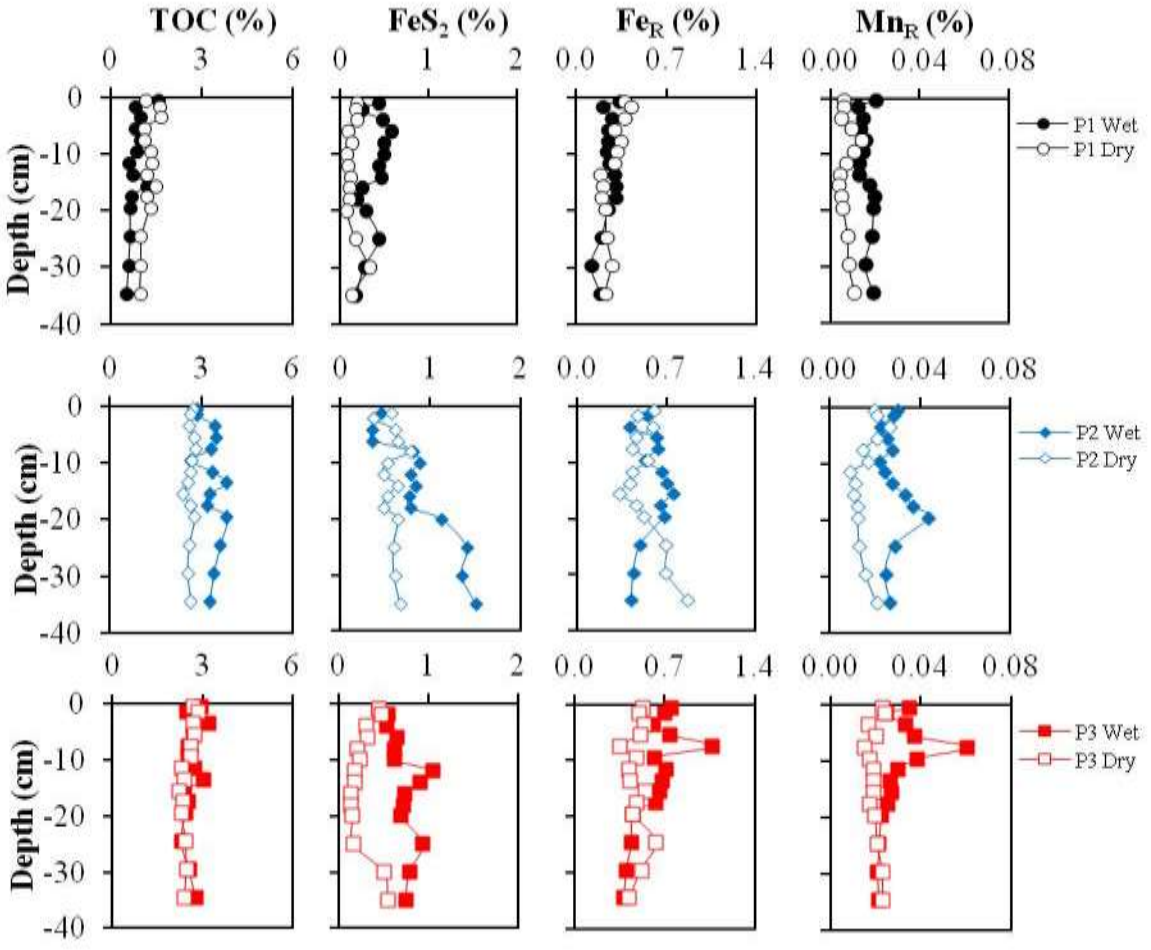

Fig. 2. Sediment TOC, FeS_2, Fe_R and Mn_R profiles at the P1 (black), P2 (blue) and P3 (red) sampling sites during the wet (solid markers) and dry (open markers) seasons.

262 *3.2 Physicochemical characteristics*

263

264 Depth salinity, pH, and Eh profiles in the overlying and pore waters in different seasons are
265 presented in Fig. 3, 4, and 5. A clear seasonal signal was noted through the upper -15 cm, with the
266 highest values detected in the dry season compared to the wet season. In the wet season, the overlying
267 water salinity was of, on average, 4, and pore water salinity increased with depth (5-20 at P1, 4-13 at
268 P2, and 4-15 at P3). In the dry season, the overlying water salinity was of, on average, 23, and pore
269 water salinity exhibited a distinct vertical pattern, decreasing with depth (24-19 at P1, 22-18 at P2
270 and 25-20 at P3). Furthermore, a significant difference between sampling sites was observed during
271 the dry and wet seasons ($p<0.05$). At P1, salinity remained constant below -18 cm in both seasons,
272 while P2 and P3 exhibited stable salinity values below -35 cm in depth.

273 pH values were slightly acidic to neutral (6.7 to 7.4), and no seasonal variations were observed
274 for the overlying water. Pore water pH values decreased with depth below the SWI during the wet
275 season. In contrast, pH values slightly increased with depth during the dry season. The determined
276 pH values were slightly more acidic during the wet season (5.9-6.5 at P1, 5.3-6.0 at P2 and 4.7-6.0 at
277 P3) compared to the dry season (6.6-7.3 at P1, 6.7-7.2 at P2 and 6.6-7.0 at P3). Eh values in the
278 overlying water were suboxic in both seasons at all sites, ranging from 40 to 190 mV. Eh values
279 dropped very strongly from the SWI and tended to decrease with depth, ranging from -357 to -80 at
280 P1, -220 to -125 at P2, and -180 to -95 at P3 in the wet season and from -146 to 0 at P1, -222 to -85
281 at P2 and, -265 to -55 at P3 in the dry season. A significant seasonal difference was noted only for P1
282 ($p<0.05$), which exhibited more reducing conditions during the wet season, and no significant
283 seasonal differences were observed for the other sites ($p>0.05$).

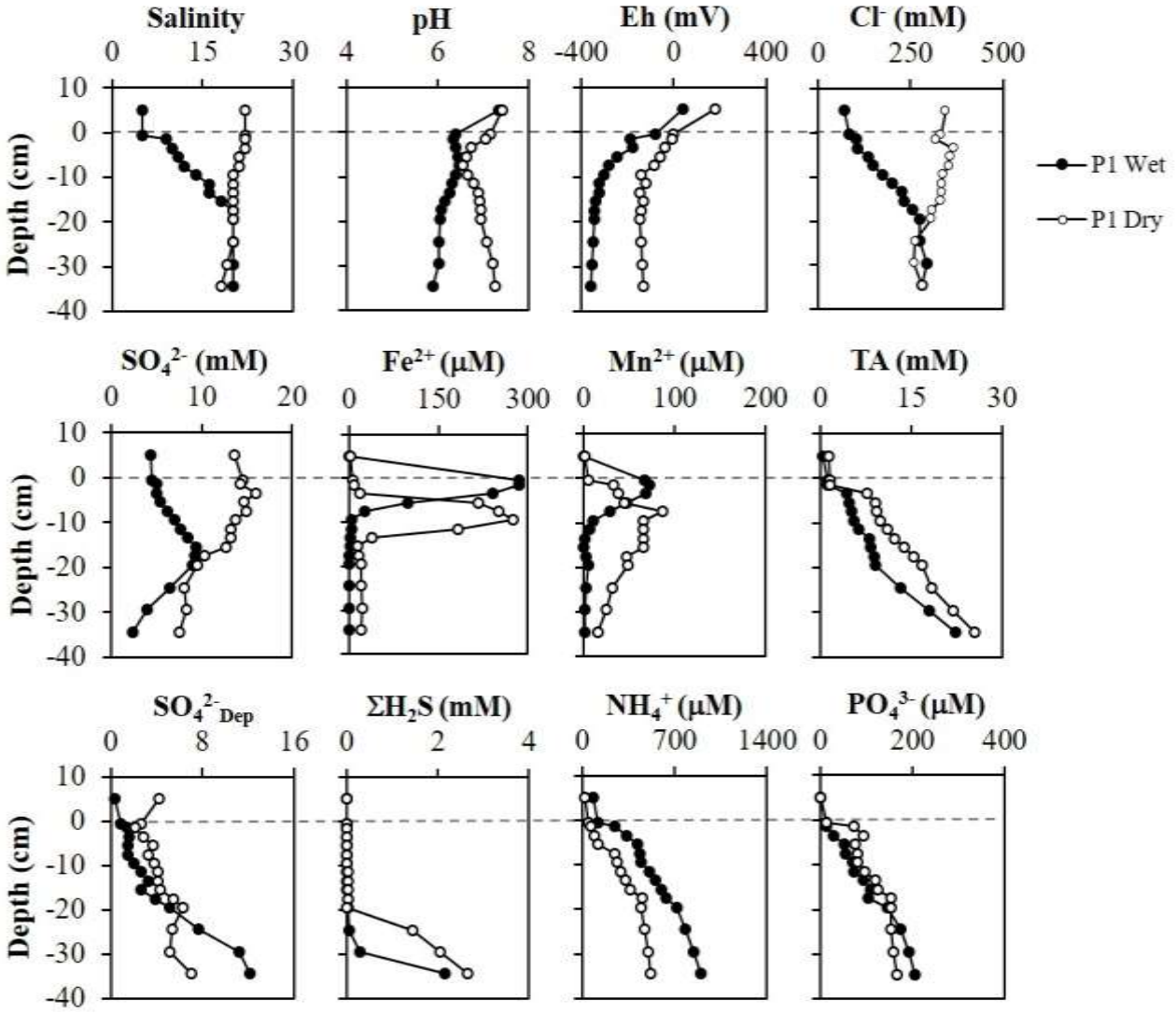

Fig. 3. Overlying and pore water profiles concerning physicochemical parameters (salinity, pH and Eh), Cl^-, SO_4^{2-}, redox-sensitive trace metals (Fe^{2+} and Mn^{2+}), total alkalinity (TA), sulfate depletion ($SO_4^{2-}{}_{Dep}$) and nutrients (NH_4^+ and PO_4^{3-}) at sampling site P1 during the wet (filled circles) and dry (open circles) seasons. Dashed horizontal lines represent the SWI.

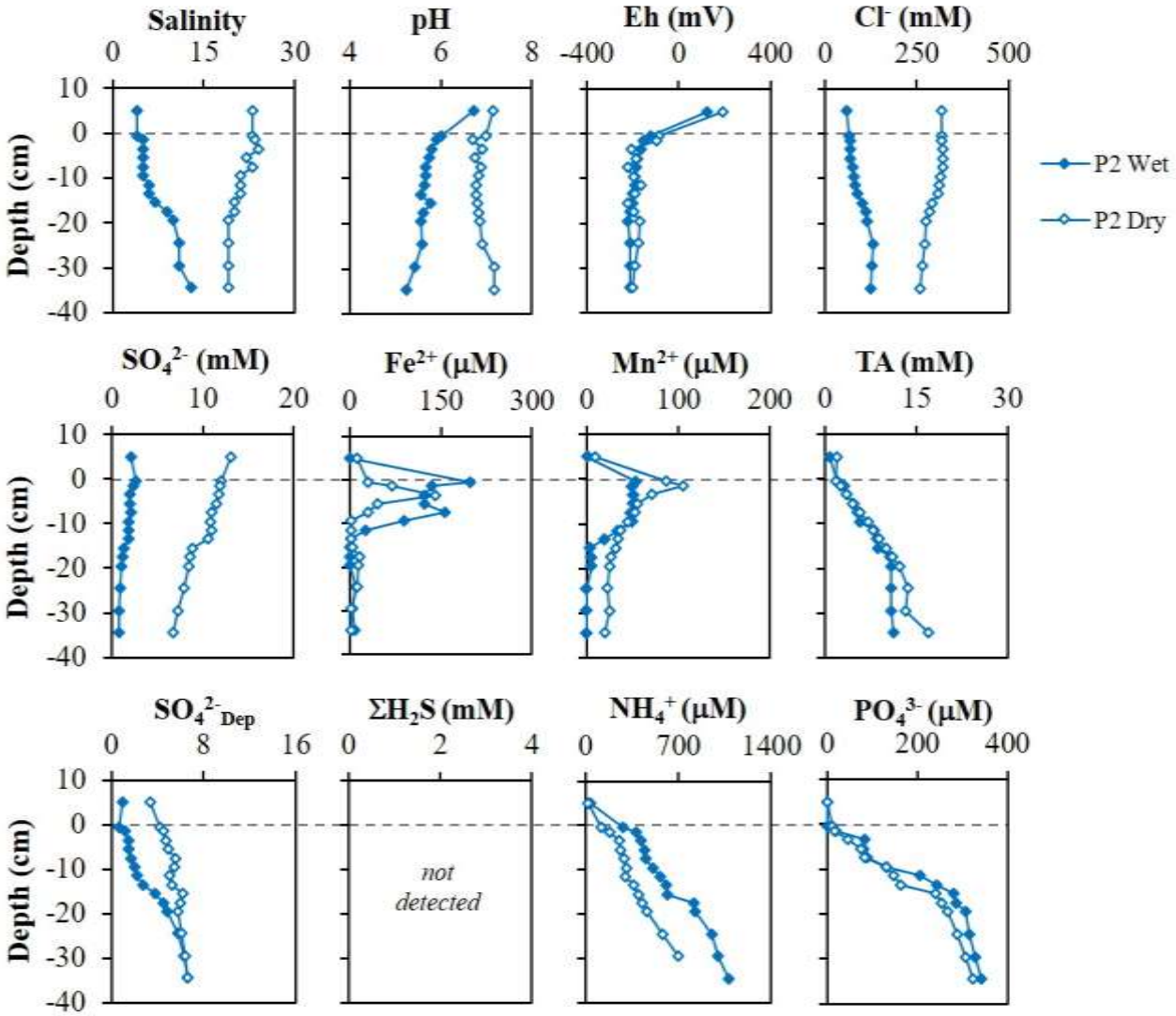

290 **Fig. 4.** Overlying and pore water profiles concerning physicochemical parameters (salinity, pH and
291 Eh), Cl^-, SO_4^{2-}, redox-sensitive trace metals (Fe^{2+} and Mn^{2+}), total alkalinity (TA), sulfate depletion
292 ($SO_4^{2-}{}_{Dep}$) and nutrients (NH_4^+ and PO_4^{3-}) at sampling site P2 during the wet (filled circles) and dry
293 (open circles) seasons. Dashed horizontal lines represent the SWI.

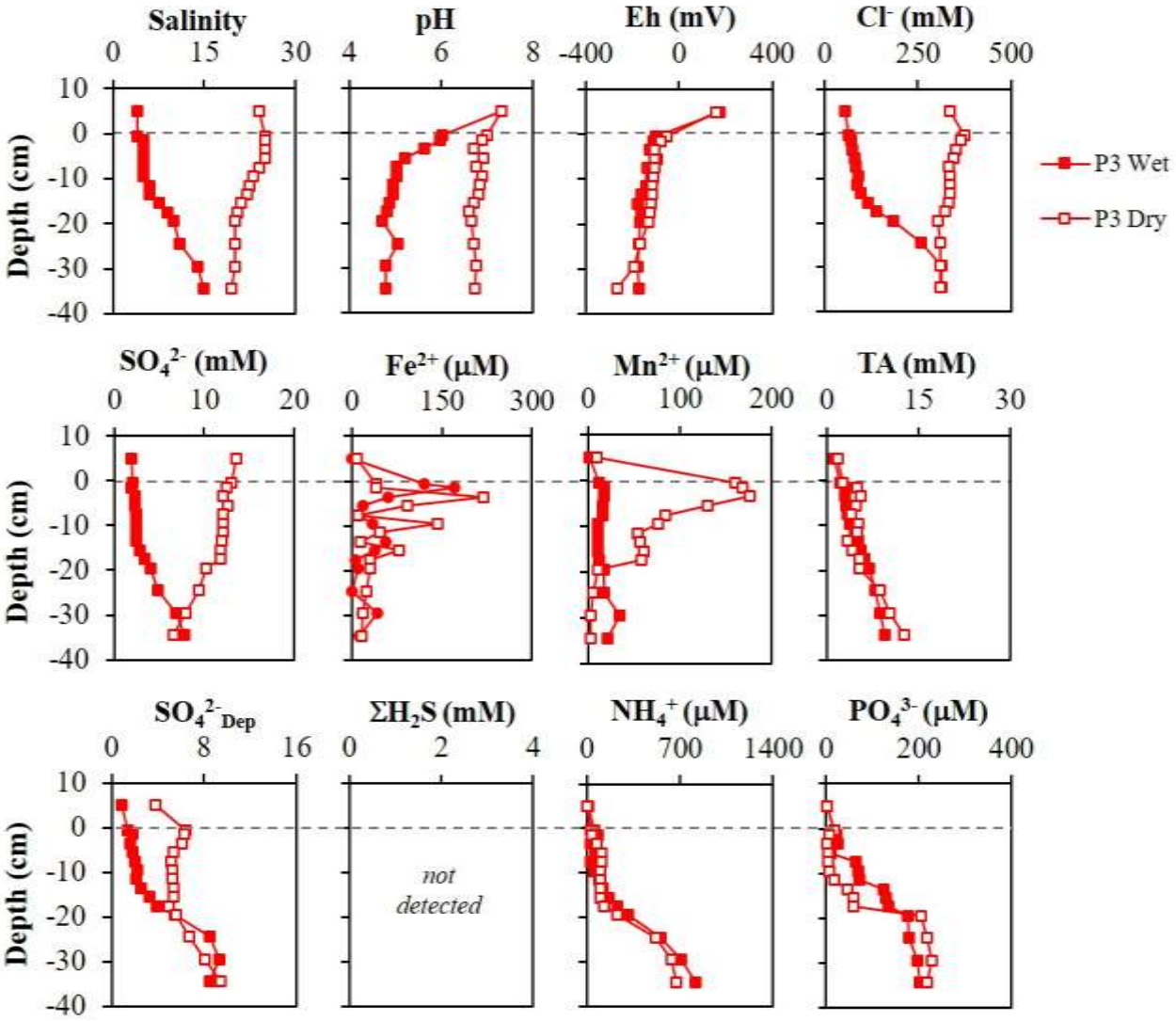

294

295 **Fig. 5.** Overlying and pore water profiles concerning physicochemical parameters (salinity, pH and
296 Eh), Cl^-, SO_4^{2-}, redox-sensitive trace metals (Fe^{2+} and Mn^{2+}), total alkalinity (TA), sulfate depletion
297 ($SO_4^{2-}{}_{Dep}$) and nutrients (NH_4^+ and PO_4^{3-}) at sampling site P3 during the wet (filled circles) and dry
298 (open circles) seasons. Dashed horizontal lines represent the SWI.

299

300 *3.3 Pore water dissolved species profiles*

301

302 Overlying and pore water profiles concerning Cl^-, SO_4^{2-}, redox-sensitive trace metals (Fe^{2+}
303 and Mn^{2+}), total alkalinity (TA), sulfate depletion ($SO_4^{2-}{}_{Dep}$), and nutrients (NH_4^+ and PO_4^{3-}) at three
304 sampling sites during the wet and dry seasons are shown in Fig. 3, 4 and 5. The Cl^- concentrations

were positively correlated with salinity values at all sites and in both seasons ($0.81 < r < 0.91$, Supplementary Table S1 and S2). At all sites, Cl^- concentrations increased from the overlying water to the pore water depth during the wet season (90-294 mM at P1, 59-143 mM at P2 and 54-314 mM at P3) and decreased with depth during the dry season (332-260 mM at P1, 317-260 mM at P2 and 376-310 mM at P3). The SO_4^{2-} concentrations exhibited a similar trend regarding salinity only during the dry season, with decreasing concentrations from the overlying water to the pore water with depth (16.0-7.5 mM at P1, 13.1-6.8 mM at P2 and 13.6-6.6 mM at P3). During the wet season, however, the downcore pore water SO_4^{2-} concentrations displayed different characteristics at each site (Fig. 3-5).

During the wet season, sites P1, P2, and P3 featured the highest pore water Fe^{2+} concentrations closer to the SWI, reaching 285.1, 198.8, and 170.1 μM, respectively. During the dry season, pore water Fe^{2+} concentrations were very low in the upper centimeters, followed by a 275 μM peak in -10 cm at site P1, 140.2 μM in -4 cm at site P2, and 219.3 μM in -4 cm at site P3. During the wet season, pore water Mn^{2+} concentrations were also higher closer to the SWI, except for P3, reaching 72.2 at site P1 and 53 μM at P2, respectively. During the dry season, Mn^{2+} peaks were located above the Fe^{2+} peaks, reaching 86.7 μM in -8 cm at site P1, 104.7 μM in -4 cm at site P2 and 175.7 μM in -4 cm at site P3. Fe^{2+} and Mn^{2+} concentrations drastically decreased below the peaks with increasing depths at the three sampling sites.

TA concentrations varied from 0.4 to 2.0 mM in the overlying water, and increased sharply with depth below the SWI, ranging from 1.1 to 25.4 mM. Pore water TA concentrations did not differ significantly between seasons ($p>0.05$). The $SO_4^{2-}{}_{Dep}$ values increased with sediment depth at all sites, ranging from 0.6 to 12.1. $SO_4^{2-}{}_{Dep}$ did not differ considerably between sites ($p>0.05$), but were significantly different between seasons at sites P2 and P3 ($p<0.05$), exhibiting slightly higher values in the dry season. Pore water ΣH_2S concentrations at P2 and P3 were negligible (<1 μM), while a high peak of 2 mM was recorded at the -35 cm depth at site P1.

330 NH_4^+ concentrations varied from 3.1 to 79.2 mM in the overlying water. The pore water NH_4^+
331 range was highest at sites P1 (119.2-900.8 μM), and P2 (286.2-1083.8 μM) compared to site P3 (72.5-
332 349.2 μM). Seasonal patterns were significant ($P<0.05$) only at P1 and P2, where pore water
333 concentrations were higher in the wet season. Pore water NH_4^+ concentrations increased with
334 sediment depth at all sites. PO_4^{3-} concentrations ranged from 0.2 to 1.0 mM in the overlying water.
335 Pore water PO_4^{3-} concentrations were not significantly different between seasons ($p>0.05$), while
336 differing significantly between sites ($p<0.05$), with the highest concentrations at P2 (1.2-342.9 μM)
337 compared to P1 (12.5-205.0 μM) and P3 (1.2-227.5 μM).
338
339 *3.4 Metal and nutrient fluxes at the sediment-water interface (SWI)*
340
341 The diffusive metal and nutrient fluxes estimates at the SWI at the three sites during the wet
342 and dry seasons are exhibited in Table 2. The Fe^{2+}, Mn^{2+}, NH_4^+, and PO_4^{3-} fluxes in both seasons at
343 all sites were positive, indicating sediment pore water exports to the overlying water. Overall, Fe^{2+},
344 Mn^{2+}, NH_4^+, and PO_4^{3-} exhibited the highest fluxes in the wet season, except for Mn^{2+} at site P3. Fe^{2+},
345 Mn^{2+}, NH_4^+, and PO_4^{3-} fluxes ranged from 6 to 723 μmol m^{2-} d^{-1}, from 16 to 189 μmol m^{2-} d^{-1}, from
346 90 to 1,433 μmol m^{2-} d^{-1}, and from 2 to 35 μmol m^{2-} d^{-1}, respectively (Table 2).
347
348 **Table 2**
349 Fe^{2+}, Mn^{2+}, NH_4^+, and PO_4^{3-} fluxes (μmol m^{-2} d^{-1}) across the SWI at sampling sites P1, P2 and P3,
350 during the wet and dry seasons.

	P1		P2		P3	
	Wet	Dry	Wet	Dry	Wet	Dry
Fe^{2+}	723	6	595	24	238	75
Mn^{2+}	92	32	73	64	16	189
NH_4^+	415	90	1,433	155	201	121
PO_4^{3-}	24	18	35	14	19	2

Positive numbers indicate fluxes from the sediment (effluxes) and negative numbers indicate fluxes to the sediment (influxes).

4 Discussion

4.1 Seasonal physicochemical properties and Cl^- variabilities

Salinity oscillations detected herein were associated to seasonal rainfall rate variations. Due to increasing rainfall rates and runoff from the Marapanim River, surface salinity values were five times lower in the wet season relative to the dry season, indicating greater saline water dilution by freshwater, as observed at the Sinnamary mangrove by Marchand et al., (2004) and at the Marapanim mangrove by Berrêdo et al., (2016). The seasonal effects controlled the conservative Cl^- and salinity values, especially in the upper sediment intervals (< 15 cm). Spatial variations were observed only during the wet season, with lower salinity and Cl^- values detected at the creek mudflats (P2 and P3) compared to the estuarine mudflat (P1). Spatial salinity and Cl^- variabilities can be explained by spatial grain size variability. The fine-grained sediments identified at P2 and P3 promote high freshwater retention capacity, while P1, characterized by sandy sediments (>50%), favored saline water recharge during rising tides. At P1, pore water salinity remained constant below -18 cm in both seasons, while pore water salinity remained constant below the -35 cm depth at P2 and P3.

The increased rainfall trend observed during the wet season led to a decrease in pH values, which may be explained by a more intense OM decomposition, as well as the reoxidation of reduced products that result in lower pH (Gueiros et al., 2003; Otero et al., 2006), such as Fe sulfide (pyrite, FeS) and pore water sulfide (HS) oxidation during the wet season. Acidity was higher at P2 and P3, reaching values lower than 5 (Fig. 4-5). These sites are located in topographically higher areas, leading to strong sediment oxidation. Sediments more acidic during the wet season have been reported in other tropical intertidal environments (Alongi et al., 2004, 1999). During the dry season, saline

377 water recharges influence pore water quality, buffering the pH close to neutrality (6.6 to 7.3), with
378 no significant difference noted between sites. Redox potential values indicate suboxic to anoxic
379 conditions at all sampling sites. Eh values were very sensitive to seasonal changes only at site P1,
380 significantly lower in the wet season than dry season (Fig. 3).
381
382 *4.2 Biogeochemical processes and seasonal variations*
383
384 Irrespective of the pathways, all mangrove OM not exported by tidal action enters the
385 sediment and is degraded or chemically modified by microorganisms (Kristensen et al., 2008).
386 Microbes in the sediment surface use electron acceptors (for example, O_2, MnO_2, Fe-oxides, SO_4^{2-})
387 in order of declining energy yields from OM respiration (Froelich et al., 1979). High OM
388 accumulation in mangrove sediments enhances intense microbial activity, sedimentary mineralization
389 rates are high, often leading to oxygen depletion within the upper few sediment millimeters (Glud,
390 2008; Kristensen et al., 1994; Meiggs and Taillefert, 2011) and favoring the prevalence of anaerobic
391 OM mineralization pathways, such as iron reduction and sulfate reduction (Alongi, 1995; Kristensen
392 et al., 2011).
393 The gradual decrease observed for TOC concentrations and redox potential with depth in all
394 sampled cores likely reflect microorganisms OM degradation. The pore water profiles allowed for
395 the assessment of the redox sequence associated to OM mangrove mudflat sediment degradation.
396 Based on downcore Fe^{2+} and Mn^{2+} variations, the sediment cores were subdivided into two distinct
397 zones, as follows: Zone 1 (from 0 to -15 cm) presents peaks with high dissolved Fe^{2+} and Mn^{2+}
398 concentrations, revealing a suboxic zone in these sediments. This mobilization is due to Fe and Mn
399 oxyhydroxides use as terminal electron acceptors in bacterial OM oxidation (Eq. 3 and 4) (Froelich
400 et al., 1979), resulting in decreased Mn_R and Fe_R concentrations (referred to in the equations as MnO_2
401 and $FeOOH/Fe(OH)_3$) in the solid-phase in this zone (Fig. 2). High Mn^{2+} and Fe^{2+} concentrations

depth sequences were recorded during the dry season, as Mn^{2+} appeared vertically in solution before Fe^{2+}. However, during the wet season, Mn^{2+} and Fe^{2+} appeared simultaneous and closer to the SWI, probably due to strong resuspension and the effect of tidal pumping caused by intense rainfall rates. Marchand et al., (2006) also observed Fe^{2+} and Mn^{2+} variations with depth associated to seasonal fluctuations.

$$236MnO_2 + (CH_2O)_{106}(NH_3)_{16}H_3PO_4 + 472H^+ \rightarrow 106HCO_3^- + 236Mn^{2+} + 8N_2 + HPO_4^{2-} + 366H_2O \quad (3)$$

$$424FeOOH + (CH_2O)_{106}(NH_3)_{16}H_3PO_4 + 756H^+ \rightarrow 424Fe^{2+} + 106HCO_3^- + 16NH_4^+ + 636H_2O + HPO_4^{2-} \quad (4)$$

Pore water Fe^{2+} reached higher concentrations at P1 (285.1 μM) compared to P2 (198.8 μM) and P3 (219.3 μM). Although freshwater discharge penetration during the wet season significantly decreased pH values, which would enhance oxyhydroxide dissolution (Holloway et al., 2016; Otero et al., 2009), the highest Fe^{2+} concentrations did not indicate significant difference between seasons, probably due to the high Fe supply from the continent (Barreiras Formation, Vilhena et al., 2010). However, Fe^{2+} peaks were typically deeper during the dry season. Low Fe^{2+} concentrations were observed at the top pore water (0 to -2 cm) during the dry season, increasing in the surface solid phase, probably due to Fe^{2+} oxidation and precipitation in the form of oxyhydroxides, likely associated to high oxygen sediment exposure during the low tide due to lower river discharges.

During tidal oscillations, multiple reduction-oxidation reactions may occur, and Fe^{2+} and Mn^{2+} may be removed from the pore water by oxidation to form oxyhydroxides (Liu et al., 2019), which explains the Fe_R and Mn_R peaks around -20 cm at P2 and -8 cm at P3 during the wet season (Fig. 2). A percentage of the dissolved Fe and Mn encounters oxygen from the sediment surface and precipitates back to Mn and Fe oxyhydroxides (Eq. 5 and 6). These peaks also seem to mark the

transition zone between suboxic and anoxic phases. Only pore water Mn^{2+} at P3 showed much lower concentrations during the wet season, consistent with higher reactive Mn_R concentrations in the solid-phase (Fig. 2). At this site, Mn_R precipitation was probably enhanced by bioturbation activities. Sediment mixing (i.e. physical or/and biological mixing) was noted in the surface sediment layers at P3, determined through the excess ^{210}Pb profiles reported by Matos et al., (2020), masking the production of pore water Mn^{2+} at the SWI. This mixing can also explain the top pore water Fe^{2+} concentration variations observed at P3. Gueiros et al., (1999) also observed higher Mn^{2+} profile intensities during the dry season compared to wet season in mudflat sediments. On the other hand, Thanh-Nho et al., (2020) and Lacerda et al., (1999) observed the highest dissolved Mn concentrations during the wet season.

$$4Fe^{2+} + 3O_2 + 6H_2O \rightarrow 4Fe(OH)_3 \quad (5)$$

$$Mn^{2+} + 1/2O_2 + 2HCO_3^- \rightarrow MnO_{2(s)} + 2CO_2 + H_2O \quad (6)$$

In zone 2 (below -15 cm), the concurrent decreases in Fe^{2+} and Mn^{2+} were accompanied by a steady increase in TA, $SO_4^{2-}{}_{dep}$, PO_4^{3-} and NH_4^+ toward the base of the core, suggesting an anoxic zone, with rapid OM mineralization in deeper sediment layers (Fig. 3-5). Regression analyses between $SO_4^{2-}{}_{Dep}$ as an estimate for the metabolic amount of sulfate reduction (SR) and TA as a terminal metabolic product were performed. According to Eq. (7), where OM is sourced from phytoplankton (Redfield et al., 1963), OM degradation is mainly related to SR. Thus, a TA:$SO_4^{2-}{}_{Dep}$ ratio of 2 would be expected. $SO_4^{2-}{}_{Dep}$ in pore waters was positively correlated to total alkalinity at all sites (see Supplementary Table S1 and S2). The TA:$SO_4^{2-}{}_{Dep}$ ratio revealed by the regression analysis slope ranged between 1.0 and 2.6. According to the Redfield ratio, this range indicates sulfate reducing conditions.

452 $(CH_2O)_{106}(NH_3)_{16}H_3PO_4 + 53SO_4^{2-} + 14H^+ \rightarrow 53H_2S + 16NH_4^+ + H_2PO_4^- + 106HCO_3^-$ (7)

453

454 Considering the pore water is devoid of free sulfide at sites P2 and P3, and appear at site P1
455 only in deeper layers, a tight coupling between sulfide production via SR and sulfide consumption by
456 pyrite formation may be proposed (Raiswell and Canfield, 1998). The ΣH_2S can react with Fe^{2+} and
457 Fe_R to form iron sulfides, e.g., FeS (Eq. 8) and FeS_2 (Eq. 9). However, the low ΣH_2S and AVS (mainly
458 FeS) concentrations can also be due to intense oxidation and pore water exchange during the air
459 exposure in the low tides. As reported by Pan et al., (2019) the formation and reoxidation of sulfide
460 in surface layers in the intertidal zones are regulated by tide-induced redox changes.

461 In the wet season, when the reducing conditions become pronounced, at sites P2 and P3 pyrite
462 concentrations increase dramatically in the solid phase below Fe^{2+} and Fe_R peaks (Fig. 2). Thus, the
463 consumption of Fe_R and Fe^{2+} in deeper sediments occurs due to iron sulfide precipitation. Lower
464 pyrite concentrations in the dry season, especially at sites P2 and P3 are probably due to these sites
465 being located in topographically higher areas and their sediments are strongly oxidized during the dry
466 season, promoting the pyrite oxidation (Eq. 10), thus Fe_R concentrations increase with depth reaching
467 higher concentrations in the dry season than the wet season in deeper sediment layers. The oxidation
468 of Fe sulfides to Fe oxyhydroxides occurred in the dry season is similar to the seasonal changes
469 observed in other studies (Luther et al., 1992; Rozan et al., 2002). Pyrite oxidation was previously
470 observed in Marapanim mangrove sediments by Vilhena et al., (2010), they observed oxidation of
471 pyrite grains surface and the presence of jarosite mineral as a product of pyrite oxidation. Mn
472 consumption at deeper layers is likely associated to pyrite coprecipitation, as reported in other
473 assessments (Huerta-Diaz, 1992; Otero and Macias, 2003; Santos-Echeandia et al., 2009).

474

475 $Fe^{2+} + 2HCO_3^- + H_2S \rightarrow FeS + 2CO_2 + H_2O$ (8)

476 $FeS + H_2S \rightarrow FeS_2 + H_2$ (9)

$$FeS_2 + 15/4O_2 + 5/2H_2O \rightarrow FeOOH + 2SO_4^{2-} + 4H^+ \quad (10)$$

Seasonal effects, mainly controlled by freshwater discharges, affected the downcore profiles of pore water $SO_4^{2-}{}_{Dep}$ in the investigated sediments. Sulfate depletion was not appreciable in the top sediment layers (above -15 cm) at all sites during the wet season, due to the dilution-mixing process, that results in a more efficient sulfate removal than bacterial SR in these layers. On the other hand, sulfate depletion increased abruptly below the dilution-mixing layers. Similar seasonal trends were also reported by Wu et al., (2015) at the Pearl River estuary. SR products (TA, NH_4^+ and PO_4^{3-}) indicated no simple mixing trend in the dilution-mixing layer (Fig. 3-5), suggesting that pore waters TA, NH_4^+ and PO_4^{3-} are substantially altered by diagenetic reactions, such as Fe and Mn reduction. However, only pore water NH_4^+ exhibited any seasonal variability, with the highest concentrations detected in the wet season. A similar phenomenon was reported by Meiggs and Taillefert, (2011), who investigated seasonal effects on estuarine sediments biogeochemical processes, indicating that dilution-mixing does not cause seasonal SR product alterations.

Suboxic to anoxic sediment conditions limit aerobic OM degradation. Iron reduction and SR are energetically less favorable degradation processes, thus enhancing OM burial. As previously observed by Matos et al., (2020), the sampling sites exhibit higher potential regarding TOC, TN and TP sediment accumulation, especially the creek mudflats (P2 and P3). The mudflat sediment in the Marapanim River margin (site P1) presented lower TOC, higher sand contents and high marine OM contributions compared to P2 and P3 (Table 1). P1, however, reached higher terminal metabolic end-products of OM mineralization concentrations, such as Fe^{2+}, $SO_4^{2-}{}_{Dep}$, H_2S and TA, suggesting that the OM of this estuarine mudflat is more susceptible to degradation compared to the mangrove creek mudflats. Typically, organic-rich sediments present high OM degradation rates. However, due to the enhanced OM and oxygen input by advective processes at the sediment surface, sandy sediments containing low organic carbon contents often exhibit OM degradation rates comparable to organic-

rich muds (Beck et al., 2008; Rusch et al., 2006). OM degradation rates further depend on sedimentary OM sources. For example, previous studies have demonstrated that marine-derived OM (fresher or more labile) is more susceptible to degradation by microorganisms than terrestrial OM (more refractory) (Hedges et al., 1997; Matos et al., 2020; Ranjan et al., 2011). Therefore, coarse-textured sediment and higher available labile OM likely contributed to more susceptible OM degradation at P1, resulting in low TOC concentrations.

4.3 Seasonal diffusive flux variability at the SWI

High amounts of Fe^{2+} and Mn^{2+} are produced by microbial Fe and Mn reduction processes, respectively, which then diffused from the sediment pore waters into the overlying water, indicating that the studied mudflats comprise a source of Fe^{2+} and Mn^{2+}. The changes in diagenetic processes induced by increasing rainfall rates, therefore, lead to variable diffusive fluxes. Concerning the wet season, the highest Fe^{2+} concentration was noted just below SWI, generating higher fluxes during this period (Table 2). One the other hand, Fe^{2+} concentrations in the dry season were lower in the top sediment layers, probably due to high oxygen sediment exposure during the low tide, enhancing oxidized solid phase severely limiting its diffusion to the overlying water. Mn^{2+} fluxes followed the same trend as Fe^{2+} fluxes, except at P3, which presented lower fluxes in the wet season due to sediment mixing, resulting lower Mn^{2+} concentrations in the surface sediment. Marchand et al. (2006) also reported higher dissolved Fe and Mn fluxes in the wet season compared to dry season, as a result of vertical redox status oscillations.

Sediment pore waters constituted a source of PO_4^{3-} and NH_4^+ to the water column at all sites, with higher fluxes in the wet compared to the dry season (Table 2). As reported by Taillardat et al. (2019), intense rainfall events reduce pore water salinity and enhance OM degradation, which is likely to increase phosphate and nitrogen mineralization. The high NH_4^+ pore water concentrations and the

527 strong correlation between NH_4^+ and $SO_4^{2-}{}_{Dep}$ pore water detected in both sampling seasons (r = 0.61
528 – 0.70, Supplementary Table S1 and S2) reveal high OM mineralization (ammonification), more
529 intense during the wet season, with higher downcore pore water concentrations. Mangrove sediments
530 generally comprise NH_4^+ sinks (Alongi, 2020b and references within), mostly due to N-NH_4^+ uptake
531 by vegetation, although an efflux for NH_4^+ is often noted (Gleeson et al., 2013; Matos et al., 2016;
532 Sadat-Noori and Glamore, 2019; Tait et al., 2017), as observed herein for the investigated mangrove
533 mudflats, as no permanent macrophytic vegetation in the mudflat is available to consume dissolved
534 nutrients (Taillardat et al., 2019).

535 Pore water PO_4^{3-} concentrations were also significantly and positively correlated with SO_4^{2-}
536 $_{Dep}$ pore water in the wet season (r = 0.64, Supplementary Table S1). This positive correlation receded
537 in the dry season (r = 0.48, Supplementary Table S2), due to enhanced $SO_4^{2-}{}_{Dep}$ in the upper layers,
538 that did not affect downcore pore water PO_4^{3-}. Other studies have indicated that the release or
539 adsorption of P in coastal sediments is associated with the iron redox cycle (Ding et al., 2016;
540 Sherman et al., 1998). Fe oxy-hydroxides potently adsorb P under more oxidizing conditions. In
541 contrast, more reducing conditions favor its mobility from sediments to pore waters (Bava and
542 Seralathan, 1999). However, low PO_4^{3-} remobilization in the upper layers where Fe reduction occurs
543 implies that PO_4^{3-} release was not associated to Fe-bound P at our investigated study sites. A low
544 negative correlation between PO_4^{3-} and Fe^{2+}, and significant positive correlations between PO_4^{3-} and
545 NH_4^+ and TA (Supplementary Table S1 and S2) reinforces the assumption that PO_4^{3-} release to pore
546 water was mainly derived from OM mineralization by SR.

547 Overall, the short but remarkable climate fluctuations influenced pore water concentrations
548 and physicochemical properties and, consequently, the intensity of metal and nutrient exchange rates
549 at the SWI in our study sites. It is, therefore, essential to take consider local weather conditions when
550 estimating and managing nutrient and metal budgets. Climatic variability (e.g., changes in rainfall
551 and the frequency and intensity of storms) can exacerbate factors affecting mangrove responses to

552 sea level, altering freshwater inflow to mangroves, sediment and nutrient inputs and salinity regime
553 (Alongi, 2018; Mcleod and Salm, 2006). Studies in Bragança Peninsula, 110 km distant from the
554 study area, indicated that mangroves have invaded higher tidal flats since 1984 due to a relative sea
555 level rise (Cohen et al., 2021, 2018, 2009; Cohen and Lara, 2003).

556 Metals and nutrients fluxes at the SWI have been estimated in other mangrove systems
557 worldwide (Supplementary Table S3), but their direction and intensity vary among sites. For example,
558 diffusive Fe^{2+} fluxes in Marapanim mangrove mudflats are low compared to temperate mangrove
559 creeks (Holloway et al., 2018; Sadat-Noori and Glamore, 2019), while diffusive Mn^{2+} fluxes present
560 the same order of magnitude as those reported for other mangrove creeks (Holloway et al., 2016; Pan
561 et al., 2019a). NH_4^+ and PO_4^{3-} fluxes are comparable to those determined in subtropical mangrove
562 forest (Kaiser et al., 2015), temperate mangrove creeks (Tait et al., 2017) and tropical mangrove-
563 fringed estuaries (Pratihary et al., 2021), but are lower than other subtropical mangrove creeks
564 (Gleeson et al., 2013; Pan et al., 2019a, 2019b) and temperate mangrove wetlands (Sadat-Noori and
565 Glamore, 2019). These variations may be due to many factors, including differences in terrestrial or
566 oceanic nutrient inputs, redox condition shifts, anthropogenic activities and local environmental
567 factors, such as weather conditions, hydrology, tidal ranges, latitudes, mangrove community
568 structures and topographic elevations (Adame et al., 2010; Adame and Lovelock, 2011; Kristensen et
569 al., 2017). In addition, this comparison must be cautiously considered, due to different analysis
570 methods and high inter-site variability.

571

572 *4.4 Pore water solute flux versus depositional fluxes*

573

574 The diffusive fluxes in mmol m^{2-} d^{-1} were converted to g m^{-2} yr^{-1} for comparisons to
575 depositional fluxes. Total nitrogen and total phosphorous depositional fluxes were obtained from
576 Matos et al. (2020). Fe and Mn depositional fluxes were estimated from reactive Fe and Mn

concentrations, sediment accumulation and dry bulk density reported previously by Matos et al., (2020). The average between the three study sites, propagate to the average between the wet and dry season dataset, of the calculated diffusive fluxes from the pore water to the overlying water column for N (as NH_4^+), P (as PO_4^{3-}), Fe (as Fe^{2+}) and Mn (as Mn^{2+}) were 2.6, 0.5, 5.7, and 1.6 g m^{-2} yr^{-1}, respectively. Regarding N, P, Fe and Mn depositional fluxes were 15.3, 3.2, 42.3 and 1.8 g m^{-2} yr^{-1}, respectively (Table 3). The release of dissolved NH_4^+, PO_4^{3-}, Fe^{2+} and Mn^{2+} from the pore water to the overlying water corresponds to averages of ~17, 16, 15 and 90 % (% recycling) of the total amount of N, P, Fe and Mn deposited in the sediment (% burial), respectively (Table 3).

Table 3

Upward diffusive NH_4^+, PO_4^{3-}, Fe^{2+} and Mn^{2+} fluxes and depositional total N and P and reactive Fe and Mn fluxes at P1, P2, and P3 sampling sites.

Site	Diffusive flux ($g\ m^{-2}\ yr^{-1}$)				Depositional flux ($g\ m^{-2}\ yr^{-1}$)				Recycling %				Burial %			
	N	P	Fe	Mn	N	P	Fe	Mn	N	P	Fe	Mn	N	P	Fe	Mn
P1	1.4	0.7	7.5	1.3	11.0	2.7	37.2	1.8	12.8	27.2	18.6	70.2	87.2	72.8	81.4	29.8
P2	5.2	0.4	6.3	1.4	16.4	3.1	42.7	1.6	31.9	11.7	18.8	86.1	68.1	88.3	81.2	13.9
P3	1.1	0.4	3.2	2.1	18.4	3.9	47.0	2.1	5.8	9.4	6.7	112.3	94.2	90.6	93.3	-12.3
Average	**2.6**	**0.5**	**5.7**	**1.6**	**15.3**	**3.2**	**42.3**	**1.8**	**16.8**	**16.1**	**14.7**	**89.5**	**83.2**	**83.9**	**85.3**	**10.5**

Marapanim mangrove sediments contain high Fe concentrations, with a mean of 6.5 % (Vilhena et al., 2010). The reactive Fe concentrations found in these mudflat sediments correspond to <10 % to those detected in the mangrove forest, highlighting Fe burial efficiency (85 %) in Marapanim mudflats. In contrast, Berrêdo et al., (2008a) observed lower total Mn concentrations (0.03%) than those detected in the investigated mudflat, of 0.06%. This high recycling potential of ~90 % corroborates with Holloway et al., (2016), who state that undisturbed mangrove creeks may be a major source of Mn^{2+} to coastal oceans. N and P burial efficiency (~84 %) is driven by suboxic

597 conditions, where Fe and Mn reductions appear to limit PO_4^{3-} and NH_4^+ pore water mobilization and
598 their fluxes to overlying surface waters.

599 Additionally to spontaneous diffusive exchange at the SWI, transport of dissolved elements
600 by advective pore water seepage and bioturbation (irrigation from burrows and biodiffusion) can also
601 be take place. Intertidal mudflat sediments are submitted to intense oscillations associated to tidal
602 heights, which may enhance nutrient and metal dissolved losses by lateral tidal drainage, advection
603 or groundwater transport (Holloway et al., 2016; Sanders et al., 2015; Tait et al., 2017). Thus, the low
604 PO_4^{3-} and NH_4^+ pore water mobilization in the upper layers can also be due to tidal-induced pore
605 water seepage from the upper layers into the creek water columns during low and ebbing tides. Pore
606 water exchange can be reduced by geochemical factors such as absorption, precipitation etc. (Ogrinc
607 and Faganeli, 2006; Rozan et al., 2002). In our study, low dissolved metal concentrations and their
608 low fluxes across the SWI during the dry season, affected by seasonal rainfall patterns, indicate
609 considerable oxidation and metals trapping into solid-phases. Bioturbation activities may increase
610 sediment oxygen supplies and a fraction of the produced Fe^{2+}, Mn^{2+} and NH_4^+ may be oxidized in the
611 upper layers where suboxic conditions can be found. On the other hand, crab burrows have been
612 demonstrated to increase the hydraulic conductivity of mangrove sediments and create a larger
613 effective surface area enhancing diffusive fluxes (Bouillon et al., 2007). Therefore, diffusive fluxes
614 based only on molecular diffusion and gradient concentrations at the SWI represent only a minimal
615 estimate of how these mudflat pore waters can act as a water column source.

616

617 **5 Conclusions**

618 The present study demonstrates that pore water concentrations, physicochemical properties,
619 and the intensity of metal and nutrient exchange rates at the SWI in intertidal mudflat sediments
620 fringed by pristine mangroves in northern Brazil are influenced by Amazonian seasonal rainfall
621 patterns. A seasonal shift from the dry to the wet season was observed, with increasing acidic and

622 reducing conditions, pore water salinity declines, and increased elemental concentrations within the
623 pore water and sediments. The redox zonation of sediments oscillated vertically in response to rainfall
624 patterns, affecting pore water species and their fluxes across the sediment-water interface. Under
625 suboxic conditions, the mudflat pore waters constitute a source of Fe^{2+}, Mn^{2+}, NH_4^+ and PO_4^{3-} to the
626 water column, and the magnitude of these effluxes increased in the wet season. However, when
627 compared with burial fluxes, the release of dissolved NH_4^+, PO_4^{3-}, Fe^{2+} and Mn^{2+} from the pore water
628 to the overlying water corresponded to ~17, 16, 7 and 90 % of the amount of TN, TP, Fe_R and Mn_R
629 deposited in the sediment, respectively. This demonstrates that Marapanim mudflats are effective in
630 retaining nutrients and Fe in their sedimentary solid phases compared to coastal water exports, while
631 also potentially comprising significant Mn contributor to coastal waters. These findings evidence the
632 role of mangrove-fringed tidal creeks as sites exhibiting intense biogeochemical processes, rather
633 than simple dissolved material routes between mangroves and coastal oceans, which are strongly
634 influenced by rainfall events.
635
636 **Acknowledgments**
637 The authors thank the research grants from the Brazilian Ministry of Education (CAPES) and the
638 Brazilian Research Council (CNPq) to the first author C.R.L. Matos. C.J. Sanders is supported by the
639 Australian Research Council (DE160100443) and E. Metzger by CNRS-EC2CO project Vubleu. W.
640 Machado thanks the CAPES-Print-Feedbacks Project (Proc. No. 88887.310301/2018-00). The
641 authors also acknowledge the Evandro Chagas Institute (IEC) and Museu Goeldi (MPEG) for the use
642 of their facilities.
643
644 **Declarations**
645 **Funding:** This work was supported in part by CAPES (Finance code 001) and by Brazilian Research
646 Council (CNPq). C.J. Sanders is supported by the Australian Research Council (DE160100443), E.

Metzger by CNRS-EC2CO project Vubleu, and W. Machado by CAPES-Print-Feedbacks Project (Proc. No. 88887.310301/2018-00).

Conflict of interest: The authors declare that they have no conflicts of interest.

Authors's contributions: All authors made substantial contributions to the conception, design, and acquisition of data. CRLM wrote first draft and all authors commented on the previous versions of the manuscript, critically revising and adding important intellectual content. All authors approved the final version.

Appendix A. Supplementary data

Supplementary data to this article can be found online at

References

Adame, M.F., Lovelock, C.E., 2011. Carbon and nutrient exchange of mangrove forests with the coastal ocean. Hydrobiologia 663, 23–50. https://doi.org/10.1007/s10750-010-0554-7

Adame, M.F., Virdis, B., Lovelock, C.E., 2010. Effect of geomorphological setting and rainfall on nutrient exchange in mangroves during tidal inundation. Mar. Freshw. Res. 61, 1197–1206. https://doi.org/10.1071/MF10013

Alongi, D.M., 2020a. Global Significance of Mangrove Blue Carbon in Climate Change Mitigation (Version 1). Sci 2, 1–15. https://doi.org/10.3390/sci2030057

Alongi, D.M., 2020b. Nitrogen Cycling and Mass Balance in the World ' s Mangrove Forests 167–189.

Alongi, D.M., 2018. Impact of global change on nutrient dynamics in Mangrove Forests. Forests 9, 1–13. https://doi.org/10.3390/f9100596

Alongi, D.M., 1995. Decomposition and recycling of organic matter in muds of the Gulf of Papua, northern Coral Sea. Cont. Shelf Res. 15, 1319–1337. https://doi.org/10.1016/0278-4343(94)00087-4

Alongi, D.M., Tirendi, F., Dixon, P., Trott, L.A., Brunskill, G.J., 1999. Mineralization of organic matter in intertidal sediments of a tropical semi-enclosed delta. Estuar. Coast. Shelf Sci. 48, 451–467. https://doi.org/10.1006/ecss.1998.0465

Alongi, D.M., Wattayakorn, G., Boyle, S., Tirendi, F., Payn, C., Dixon, P., 2004. Influence of roots and climate on mineral and trace element storage and flux in tropical mangrove soils. Biogeochemistry 69, 105–123. https://doi.org/10.1023/B:BIOG.0000031043.06245.af

Alongi, D.M., Wattayakorn, G., Pfitzner, J., Tirendi, F., Zagorskis, I., Brunskill, G.J., Davidson, A., Clough, B.F., 2001. Organic carbon accumulation and metabolic pathways in sediments of mangrove forests in southern Thailand. Mar. Geol. 179, 85–103. https://doi.org/10.1016/S0025-3227(01)00195-5

Anschutz, P., Dedieu, K., Desmazes, F., Chaillou, G., 2005. Speciation, oxidation state, and reactivity of particulate manganese in marine sediments. Chem. Geol. 218, 265–279. https://doi.org/10.1016/j.chemgeo.2005.01.008

Bally, G., Mesnage, V., Deloffre, J., Clarisse, O., Lafite, R., Dupont, J.P., 2004. Chemical

687 characterization of porewaters in an intertidal mudflat of the Seine estuary: Relationship to
688 erosion-deposition cycles. Mar. Pollut. Bull. 49, 163–173.
689 https://doi.org/10.1016/j.marpolbul.2004.02.005
690 Bava, K.A., Seralathan, P., 1999. Interstitial water and hydrochemistry of a mangrove forest and
691 adjoining water system , south west coast of India. Environ. Geol. 38, 47–52.
692 Beck, M., Dellwig, O., Liebezeit, G., Schnetger, B., 2008. Spatial and seasonal variations of
693 sulphate, dissolved organic carbon, and nutrients in deep pore waters of intertidal flat
694 sediments. Estuar. , Coast. Shelf Sci. 79, 307–316. https://doi.org/10.1016/j.ecss.2008.04.007
695 Berner, R.A., 1980. Early Diagenesis - A Theorical Approch. Princeton University Press, New
696 Jersey.
697 Berrêdo, J.F., Costa, M.L. da, Vilhena, M. do P.S.P., Santos, J.T. dos, 2008a. Mineralogia e
698 geoquímica de sedimentos de manguezais da costa amazônica: o exemplo do estuário do rio
699 Marapanim (Pará). Rev. Bras. Geociências 38, 24–35. https://doi.org/10.25249/0375-
700 7536.20083812435
701 Berrêdo, J.F., Costa, M.L. da, Vilhena, M.S.P., Matos, C.R.L., 2016. Modificações nas
702 propriedades físico-químicas de sedimentos de manguezais submetidos ao clima amazônico
703 Changes in physicochemical properties of mangrove sediments under Amazonian climatic
704 regime. Bol. do Mus. Para. Emílio Goeldi Ciências Nat. 11, 313–328.
705 Berrêdo, J.F., Costa, M.L., Socorro, P., 2008b. Efeitos das variações sazonais do clima tropical
706 úmido sobre as águas e sedimentos de manguezais do estuário do rio Marapanim , costa
707 nordeste do Estado do Pará. Acta Amaz. 38, 473–482.
708 https://doi.org/http://dx.doi.org/10.1590/S0044-59672008000300012
709 Bouillon, S., Middelburg, J.J., Dehairs, F., Borges, A. V., Abril, G., Flindt, M.R., Ulomi, S.,
710 Kristensen, E., 2007. Importance of intertidal intertidal sediment processes and porewater
711 exchange on the water column biogeochemistry in a pristine mangrove creek (Ras Dege,
712 Tanzania). Biogeosciences 4, 311–322. https://doi.org/10.5194/bg-4-311-2007
713 Breithaupt, J.L., Smoak, J.M., Smith III, T.J., Sanders, C.J., 2014. Temporal variability of carbon
714 and nutrient burial, sediment accretion, and mass accumulation over the past century in a
715 carbonate platform mangrove forest of the Florida Everglades. J. Geophys. Res. Biogeosci.
716 119, 2032–2048. https://doi.org/10.1002/2014JG002715.Received
717 Cline, J.D., 1969. SPECTROPHOTOMETRIC DETERMINATION OF HYDROGEN SULFIDE
718 IN NATURAL WATERS1. Limnol. Oceanogr. 14, 454–458.
719 https://doi.org/10.4319/lo.1969.14.3.0454
720 Cohen, M.C.L., Behling, H., Lara, R.J., Smith, C.B., Matos, H.R.S., Vedel, V., 2009. Impact of sea-
721 level and climatic changes on the Amazon coastal wetlands during the late Holocene. Veg.
722 Hist. Archaeobot. 18, 425–439. https://doi.org/10.1007/s00334-008-0208-0
723 Cohen, M.C.L., Camargo, P.M.P., Pessenda, L.C.R., Lorente, F.L., De Souza, A. V., Corrêa,
724 J.A.M., Bendassolli, J., Dietz, M., 2021. Effects of the middle Holocene high sea-level stand
725 and climate on Amazonian mangroves. J. Quat. Sci. 36, 1013–1027.
726 https://doi.org/10.1002/jqs.3343
727 Cohen, M.C.L., de Souza, A. V., Rossetti, D.F., Pessenda, L.C.R., França, M.C., 2018. Decadal-
728 scale dynamics of an Amazonian mangrove caused by climate and sea level changes:
729 Inferences from spatial-temporal analysis and digital elevation models. Earth Surf. Process.
730 Landforms 43, 2876–2888. https://doi.org/10.1002/esp.4440
731 Cohen, M.C.L., Lara, R.J., 2003. Temporal changes of mangrove vegetation boundaries in
732 Amazonia: Application of GIS and remote sensing techniques. Wetl. Ecol. Manag. 11, 223–
733 231. https://doi.org/10.1023/A:1025007331075
734 Ding, S., Wang, Y., Wang, D., Li, Y.Y., Gong, M., Zhang, C., 2016. In situ , high-resolution
735 evidence for iron-coupled mobilization of phosphorus in sediments. Nat. Publ. Gr. 1–11.
736 https://doi.org/10.1038/srep24341

737 Dittmar, T., Hertkorn, N., Kattner, G., Lara, R.J., 2006. Mangroves, a major source of dissolved
738 organic carbon to the oceans. Global Biogeochem. Cycles 20, 1–7.
739 https://doi.org/10.1029/2005GB002570
740 Dittmar, T., Lara, R.J., 2001. Driving forces behind nutrient and organic matter dynamics in a
741 mangrove tidal creek in North Brazil. Estuar. Coast. Shelf Sci. 52, 249–259.
742 https://doi.org/10.1006/ecss.2000.0743
743 Fossing, H., Jørgensen, B., 1989. Measurement of bacterial sulfate reduction in sediments:
744 Evaluation of a single-step chromium reduction method. Biogeochemistry 8, 205–222.
745 https://doi.org/10.1007/BF00002889
746 Froelich, P.N., Klinkhammer, G.P., Bender, M.L., Luedtke, N.A., Heath, G.R., Cullen, D.,
747 Dauphin, P., Hammond, D., Hartman, B., Maynard, V., 1979. Early oxidation of organic
748 matter in pelagic sediments of the eastern equatorial Atlantic: suboxic diagenesis. Geochim.
749 Cosmochim. Acta 43, 1075–1090. https://doi.org/10.1016/0016-7037(79)90095-4
750 Gieskes, J.M., Gamo, T., Brumsack, H., 1991. Chemical Methods for Interstitial Water Analysis
751 aboard JOIDES Resolution, College Station, Texas, Ocean DrillingProgram. ODP Tech. Note.
752 https://doi.org/10.2973/odp.tn.15.1991
753 Gleeson, J., Santos, I.R., Maher, D.T., Golsby-Smith, L., 2013. Groundwater-surface water
754 exchange in a mangrove tidal creek: Evidence from natural geochemical tracers and
755 implications for nutrient budgets. Mar. Chem. 156, 27–37.
756 https://doi.org/10.1016/j.marchem.2013.02.001
757 Glud, R.N., 2008. Oxygen dynamics of marine sediments. Mar. Biol. Res. 4, 243–289.
758 https://doi.org/10.1080/17451000801888726
759 Gueiros, B.B., Machado, W., Filho, S.D.L., Lacerda, L.D., 2003. Manganese behavior at the
760 sediment-water interface in a mangrove dominated area in Sepetiba Bay, SE Brazil. J. Coast.
761 Res. 19, 550–559.
762 Hammer, Ø., Harper, D.A.T., Ryan, P.D., 2001. PAST : PALEONTOLOGICAL STATISTICS
763 SOFTWARE PACKAGE FOR EDUCATION AND DATA ANALYSIS. Palaeontol. Electron.
764 4, 1–9.
765 Hedges, J.I., Keil, R.G., Benner, R., 1997. What happens to terrestrial organic matter in the ocean ?
766 Org. Geochem. 27, 195–212. https://doi.org/https://doi.org/10.1016/S0146-6380(97)00066-1
767 Holloway, C.J., Santos, I.R., Rose, A.L., 2018. Porewater inputs drive Fe redox cycling in the water
768 column of a temperate mangrove wetland. Estuar. Coast. Shelf Sci. 207, 259–268.
769 https://doi.org/10.1016/j.ecss.2018.04.016
770 Holloway, C.J., Santos, I.R., Tait, D.R., Sanders, C.J., Rose, A.L., Schnetger, B., Brumsack, H.J.,
771 Macklin, P.A., Sippo, J.Z., Maher, D.T., 2016. Manganese and iron release from mangrove
772 porewaters: A significant component of oceanic budgets? Mar. Chem. 184, 43–52.
773 https://doi.org/10.1016/j.marchem.2016.05.013
774 Huerta-Diaz J.W., M.A.A.-M., 1992. Pyritization of trace metals in anoxic marine sediments: RN -
775 Geochim. Cosmochim. Acta, v. 56, p. 2681-2702. Geochim. Cosmochim. Acta 56.
776 Jennerjahn, T.C., Ittekkot, V., 2002. Relevance of mangroves for the production and deposition of
777 organic matter along tropical continental margins. Naturwissenschaften 89, 23–30.
778 https://doi.org/10.1007/s00114-001-0283-x
779 Kaiser, D., Kowalski, N., Böttcher, M.E., Yan, B., Unger, D., 2015. Benthic nutrient fluxes from
780 mangrove sediments of an anthropogenically impacted estuary in Southern China. J. Mar. Sci.
781 Eng. 3, 466–491. https://doi.org/10.3390/jmse3020466
782 Kauffman, J.B., Bernardino, A.F., Ferreira, T.O., Giovannoni, L.R., De Gomes, L.E.O., Romero,
783 D.J., Jimenez, L.C.Z., Ruiz, F., 2018. Carbon stocks of mangroves and salt marshes of the
784 Amazon region, Brazil. Biol. Lett. 14. https://doi.org/10.1098/rsbl.2018.0208
785 Kostka, J.E., Luther, G.W., 1994. Partitioning and speciation of solid phase iron in saltmarsh
786 sediments. Geochim. Cosmochim. Acta 58, 1701–1710. https://doi.org/10.1016/0016-

787 7037(94)90531-2
788 Kristensen, E., Bouillon, S., Dittmar, T., Marchand, C., 2008. Organic carbon dynamics in
789 mangrove ecosystems : A review. Aquat. Bot. 89, 201–219.
790 https://doi.org/10.1016/j.aquabot.2007.12.005
791 Kristensen, E., Connolly, R.M., Otero, X.L., Marchand, C., Ferreira, T.O., Rivera-Monroy, V.H.,
792 2017. Biogeochemical cycles: Global approaches and perspectives, Mangrove Ecosystems: A
793 Global Biogeographic Perspective: Structure, Function, and Services.
794 https://doi.org/10.1007/978-3-319-62206-4_6
795 Kristensen, E., King, G., Holmer, M., Banta, G., Jensen, M., Hansen, K., Bussarawit, N., 1994.
796 Sulfate reduction, acetate turnover and carbon metabolism in sediments of the Ao Nam Bor
797 mangrove, Phuket, Thailand. Mar. Ecol. Prog. Ser. 111, 245–255.
798 https://doi.org/10.3354/meps111245
799 Kristensen, E., Mangion, P., Tang, M., Flindt, M.R., Holmer, M., Ulomi, S., 2011. Microbial
800 carbon oxidation rates and pathways in sediments of two Tanzanian mangrove forests.
801 Biogeochemistry 103, 143–158. https://doi.org/10.1007/s10533-010-9453-2
802 Lacerda, L.D., Jr, M.G.R., Gueiros, B.B., 1999. Manganese dynamics in a mangrove mud flat tidal
803 creek in SE Brazil 100, 105–115.
804 Lee, R.Y., Porubsky, W.P., Feller, I.C., McKee, K.L., Joye, S.B., 2008. Porewater biogeochemistry
805 and soil metabolism in dwarf red mangrove habitats (Twin Cays, Belize). Biogeochemistry 87,
806 181–198. https://doi.org/10.1007/s10533-008-9176-9
807 Li, Y.-H., Gregory, S., 1974. Diffusion of ions in sea water and in deep-sea sediments. Geochim.
808 Cosmochim. Acta 38, 703–714. https://doi.org/10.1016/0016-7037(74)90145-8
809 Liu, Y., Not, C., Jiao, J.J., Liang, W., Lu, M., 2019. Tidal induced dynamics and geochemical
810 reactions of trace metals (Fe, Mn, and Sr) in the salinity transition zone of an intertidal aquifer.
811 Sci. Total Environ. 664, 1133–1149. https://doi.org/10.1016/j.scitotenv.2019.01.374
812 Luther, G.W., Kostka, J.E., Church, T.M., Sulzberger, B., Stumm, W., 1992. Seasonal iron cycling
813 in the salt-marsh sedimentary environment: the importance of ligand complexes with Fe(II)
814 and Fe(III) in the dissolution of Fe(III) minerals and pyrite, respectively. Mar. Chem. 40, 81–
815 103. https://doi.org/10.1016/0304-4203(92)90049-G
816 Marchand, C., Baltzer, F., Lallier-Vergès, E., Albéric, P., 2004. Pore-water chemistry in mangrove
817 sediments: Relationship with species composition and developmental stages (French Guiana).
818 Mar. Geol. 208, 361–381. https://doi.org/10.1016/j.margeo.2004.04.015
819 Marchand, C., Lallier-Vergès, E., Allenbach, M., 2011. Redox conditions and heavy metals
820 distribution in mangrove forests receiving effluents from shrimp farms (Teremba Bay, New
821 Caledonia). J. Soils Sediments 11, 529–541. https://doi.org/10.1007/s11368-010-0330-3
822 Marchand, C., Lallier-Vergès, E., Baltzer, F., Albéric, P., Cossa, D., Baillif, P., 2006. Heavy metals
823 distribution in mangrove sediments along the mobile coastline of French Guiana. Mar. Chem.
824 98, 1–17. https://doi.org/10.1016/j.marchem.2005.06.001
825 Matos, C.R.L., Berrêdo, J.F., Machado, W., Sanders, C.J., Metzger, E., Cohen, M.C.L., 2020.
826 Carbon and nutrient accumulation in tropical mangrove creeks, Amazon region. Mar. Geol.
827 429. https://doi.org/10.1016/j.margeo.2020.106317
828 Matos, C.R.L., Mendoza, U., Diaz, R., Moreira, M., Belem, A.L., Metzger, E., Albuquerque,
829 A.L.S., Machado, W., 2016. Nutrient regeneration susceptibility under contrasting sedimentary
830 conditions from the Rio de Janeiro coast, Brazil. Mar. Pollut. Bull. 108.
831 https://doi.org/10.1016/j.marpolbul.2016.04.046
832 Mcleod, E., Salm, R. V, 2006. Managing Mangroves for Resilience to Climate Change IUCN
833 Global Marine Programme, Iucn.
834 Meiggs, D., Taillefert, M., 2011. The effect of riverine discharge on biogeochemical processes in
835 estuarine sediments. Limnol. Oceanogr. 56, 1797–1810.
836 https://doi.org/10.4319/lo.2011.56.5.1797

837 Nascimento, W.R., Wal, P., Proisy, C., Lucas, R.M., 2013. Estuarine , Coastal and Shelf Science
838 Mapping changes in the largest continuous Amazonian mangrove belt using object-based
839 classi fi cation of multisensor satellite imagery. Estuar. Coast. Shelf Sci. 117, 83–93.
840 https://doi.org/10.1016/j.ecss.2012.10.005
841 Ogrinc, N., Faganeli, J., 2006. Phosphorus regeneration and burial in near-shore marine sediments
842 (the Gulf of Trieste, northern Adriatic Sea). Estuar. Coast. Shelf Sci. 67, 579–588.
843 https://doi.org/10.1016/j.ecss.2005.12.016
844 Otero, X.L., Ferreira, T.O., Huerta-Díaz, M.A., Partiti, C.S.M., Souza, V., Vidal-Torrado, P.,
845 Macías, F., 2009. Geochemistry of iron and manganese in soils and sediments of a mangrove
846 system, Island of Pai Matos (Cananeia - SP, Brazil). Geoderma 148, 318–335.
847 https://doi.org/10.1016/j.geoderma.2008.10.016
848 Otero, X.L., Ferreira, T.O., Vidal-Torrado, P., Macías, F., 2006. Spatial variation in pore water
849 geochemistry in a mangrove system (Pai Matos island , Cananeia-Brazil). Appl.
850 Geochemistry 21, 2171–2186. https://doi.org/10.1016/j.apgeochem.2006.07.012
851 Otero, X.L., Macias, F., 2003. Spatial variation in pyritization of trace metals in salt-marsh soils.
852 Biogeochemistry 62, 59–86. https://doi.org/10.1023/A:1021115211165
853 Ovalle, A.R.C., Rezende, C.E., Lacerda, L.D., Silva, C.A.R., 1990. Factors affecting the
854 hydrochemistry of a mangrove tidal creek, sepetiba bay, Brazil. Estuar. Coast. Shelf Sci. 31,
855 639–650. https://doi.org/10.1016/0272-7714(90)90017-L
856 Pan, F., Guo, Z., Cai, Y., Fu, Y., Wu, J., Wang, B., Liu, H., Gao, A., 2020. Cyclical patterns and
857 (im)mobilization mechanisms of phosphorus in sediments from a small creek estuary:
858 Evidence from in situ monthly sampling and indoor experiments. Water Res. 171, 115479.
859 https://doi.org/10.1016/j.watres.2020.115479
860 Pan, F., Liu, H., Guo, Z., Cai, Y., Fu, Y., Wu, J., Wang, B., 2019a. Metal/metalloid and phosphorus
861 characteristics in porewater associated with manganese geochemistry : A case study in the
862 Jiulong River Estuary, China. Environ. Pollut. 255, 113134.
863 https://doi.org/10.1016/j.envpol.2019.113134
864 Pan, F., Liu, H., Guo, Z., Li, Z., Wang, B., Cai, Y., Gao, A., 2019b. Effects of tide and season
865 changes on the iron-sulfur-phosphorus biogeochemistry in sediment porewater of a mangrove
866 coast. J. Hydrol. 568, 686–702. https://doi.org/10.1016/j.jhydrol.2018.11.002
867 Pratihary, A., Naik, R., Karapurkar, S., Gauthankar, M., Khandeparker, R., Manjrekar, S., Gauns,
868 M., 2021. Benthic exchange along a tropical estuarine salinity gradient during dry season:
869 Biogeochemical and ecological implications. J. Sea Res. 177, 102124.
870 https://doi.org/10.1016/j.seares.2021.102124
871 Raiswell, R., Canfield, D.E., 1998. Sources of iron for pyrite formation in marine sediments. Am. J.
872 Sci. 298, 219–245. https://doi.org/10.2475/ajs.298.3.219
873 Ranjan, R.L., Routh, J., Ramanathan, A.L., Klump, J.V., 2011. Elemental and stable isotope records
874 of organic matter input and its fate in the Pichavaram mangrove – estuarine sediments (Tamil
875 Nadu , India). Mar. Chem. 126, 163–172. https://doi.org/10.1016/j.marchem.2011.05.005
876 Rao, K., Priya, N., Ramanathan, A.L., 2018. Impact of seasonality on the nutrient concentrations in
877 Gautami-Godavari Estuarine Mangrove Complex, Andhra Pradesh, India. Mar. Pollut. Bull.
878 129, 329–335. https://doi.org/10.1016/j.marpolbul.2018.02.052
879 Redfield, A.C., Ketchum, B.H., Richards, A., 1963. The influence of organisms on the composition
880 of sea water., in: Hill, M.M. (Ed.), The Sea. Interscience, Geneva, pp. 26–77.
881 Rozan, T.F., Taillefert, M., Trouwborst, R.E., Glazer, B.T., Ma, S., Herszage, J., Valdes, L.M.,
882 Price, K.S., Luther, G.W., 2002. Iron-sulfur-phosphorus cycling in the sediments of a shallow
883 coastal bay: Implications for sediment nutrient release and benthic macroalgal blooms. Limnol.
884 Oceanogr. 47, 1346–1354. https://doi.org/10.4319/lo.2002.47.5.1346
885 Rusch, A., Huettel, M., Wild, C., Reimers, C.E., 2006. Benthic Oxygen Consumption and Organic
886 Matter Turnover in Organic-poor , Permeable Shelf Sands. Aquat. Geochemistry 12, 1–19.

887 https://doi.org/10.1007/s10498-005-0784-x
888 Sadat-Noori, M., Glamore, W., 2019. Porewater exchange drives trace metal, dissolved organic
889 carbon and total dissolved nitrogen export from a temperate mangrove wetland. J. Environ.
890 Manage. 248, 109264. https://doi.org/10.1016/j.jenvman.2019.109264
891 Sanders, C.J., Eyre, B.D., Santos, I.R., Machado, W., Luiz-silva, W., Smoak, J.M., Breithaupt, J.L.,
892 Ketterer, M.E., Sanders, L., Marotta, H., Silva-filho, E., Al, S.E.T., 2014. impacted mangrove
893 wetland. Geophys. Res. Lett. 2475–2480. https://doi.org/10.1002/2014GL059789.Received
894 Sanders, C.J., Santos, I.R., Maher, D.T., Sadat-Noori, M., Schnetger, B., Brumsack, H.J., 2015.
895 Dissolved iron exports from an estuary surrounded by coastal wetlands: Can small estuaries be
896 a significant source of Fe to the ocean? Mar. Chem. 176, 75–82.
897 https://doi.org/10.1016/j.marchem.2015.07.009
898 Santos-Echeandia, J., Prego, R., Cobelo-García, A., Millward, G.E., 2009. Porewater geochemistry
899 in a Galician Ria (NW Iberian Peninsula): Implications for benthic fluxes of dissolved trace
900 elements (Co, Cu, Ni, Pb, V, Zn). Mar. Chem. 117, 77–87.
901 https://doi.org/10.1016/j.marchem.2009.05.001
902 Seeberg-Elverfeldt, J., Schlüter, M., Feseker, T., Kölling, M., 2005. Rhizon sampling of porewaters
903 near the sediment-water interface of aquatic systems. Limnol. Oceanogr. Methods 3, 361–371.
904 https://doi.org/10.4319/lom.2005.3.361
905 Sherman, R.E., Fahey, T.J., Howarth, R.W., 1998. Soil-plant interactions in a neotropical mangrove
906 forest: Iron, phosphorus and sulfur dynamics. Oecologia.
907 https://doi.org/10.1007/s004420050553
908 Silva, C.A. da, Souza-Filho, P.W.M., Rodrigues, S.W.P., 2009. Morphology and modern
909 sedimentary deposits of the macrotidal Marapanim Estuary (Amazon, Brazil). Cont. Shelf Res.
910 29, 619–631. https://doi.org/10.1016/j.csr.2008.09.018
911 Taillardat, P., Ziegler, A.D., Friess, D.A., Widory, D., David, F., Ohte, N., Nakamura, T., Evaristo,
912 J., Thanh-Nho, N., Van Vinh, T., Marchand, C., 2019. Assessing nutrient dynamics in
913 mangrove porewater and adjacent tidal creek using nitrate dual-stable isotopes: A new
914 approach to challenge the Outwelling Hypothesis? Mar. Chem. 214, 103662.
915 https://doi.org/10.1016/j.marchem.2019.103662
916 Tait, D.R., Maher, D.T., Sanders, C.J., Santos, I.R., 2017. Radium-derived porewater exchange and
917 dissolved N and P fluxes in mangroves. Geochim. Cosmochim. Acta 200, 295–309.
918 https://doi.org/10.1016/j.gca.2016.12.024
919 Terada, K., Koibuchi, Y., Isobe, M., 2017. Rainfall effect on sediment and nutrient fluxes in a small
920 mangrove river, Okinawa, Japan. J. Mar. Res. 75, 1–17.
921 https://doi.org/10.1357/002224017821219027
922 Thanh-Nho, N., Marchand, C., Strady, E., Van Vinh, T., Taillardat, P., Cong-Hau, N., Nhu-Trang,
923 T.T., 2020. Trace Metal Dynamics in a Tropical Mangrove Tidal Creek: Influence of
924 Porewater Seepage (Can Gio, Vietnam). Front. Environ. Sci. 8.
925 https://doi.org/10.3389/fenvs.2020.00139
926 Thanh-Nho, N., Marchand, C., Strady, E., Vinh, T. Van, Nhu-Trang, T.T., 2019. Metals
927 geochemistry and ecological risk assessment in a tropical mangrove (Can Gio, Vietnam).
928 Chemosphere 219, 365–382. https://doi.org/10.1016/j.chemosphere.2018.11.163
929 Thibault de Chanvalon, A., Metzger, E., Mouret, A., Knoery, J., Geslin, E., Meysman, F.J.R., 2017.
930 Two dimensional mapping of iron release in marine sediments at submillimetre scale. Mar.
931 Chem. 191, 34–49. https://doi.org/10.1016/j.marchem.2016.04.003
932 Vilhena, M.D.P.S.P., Costa, M.L. Da, Berrêdo, J.F., 2010. Continental and marine contributions to
933 formation of mangrove sediments in an Eastern Amazonian mudplain: The case of the
934 Marapanim Estuary. J. South Am. Earth Sci. 29, 427–438.
935 https://doi.org/10.1016/j.jsames.2009.07.005
936 Wang, W.W., Li, D.J., Zhou, J.L., Gao, L., 2011. Nutrient dynamics in pore water of tidal marshes

near the Yangtze Estuary and Hangzhou Bay, China. Environ. Earth Sci. 63, 1067–1077. https://doi.org/10.1007/s12665-010-0782-1

Weston, N.B., Porubsky, W.P., Samarkin, V.A., Erickson, M., Macavoy, S.E., Joye, S.B., 2006. Porewater stoichiometry of terminal metabolic products, sulfate, and dissolved organic carbon and nitrogen in estuarine intertidal creek-bank sediments. Biogeochemistry 77, 375–408. https://doi.org/10.1007/s10533-005-1640-1

Wu, Z., Zhou, H., Ren, D., Gao, H., Li, J., 2015. Processes controlling the seasonal and spatial variations in sulfate profiles in the pore water of the sediments surrounding Qi'ao Island, Pearl River Estuary, Southern China. Cont. Shelf Res. 98, 26–35. https://doi.org/10.1016/j.csr.2015.02.001

Yasui, S., Kanda, J., Usui, T., Ogawa, H., 2016. Seasonal variations of dissolved organic matter and nutrients in sediment pore water in the inner part of Tokyo Bay. J. Oceanogr. 72, 851–866. https://doi.org/10.1007/s10872-016-0382-0